

Updates from GWTC-5 and latest results from the search for an Isotropic GWB from LVK's O4

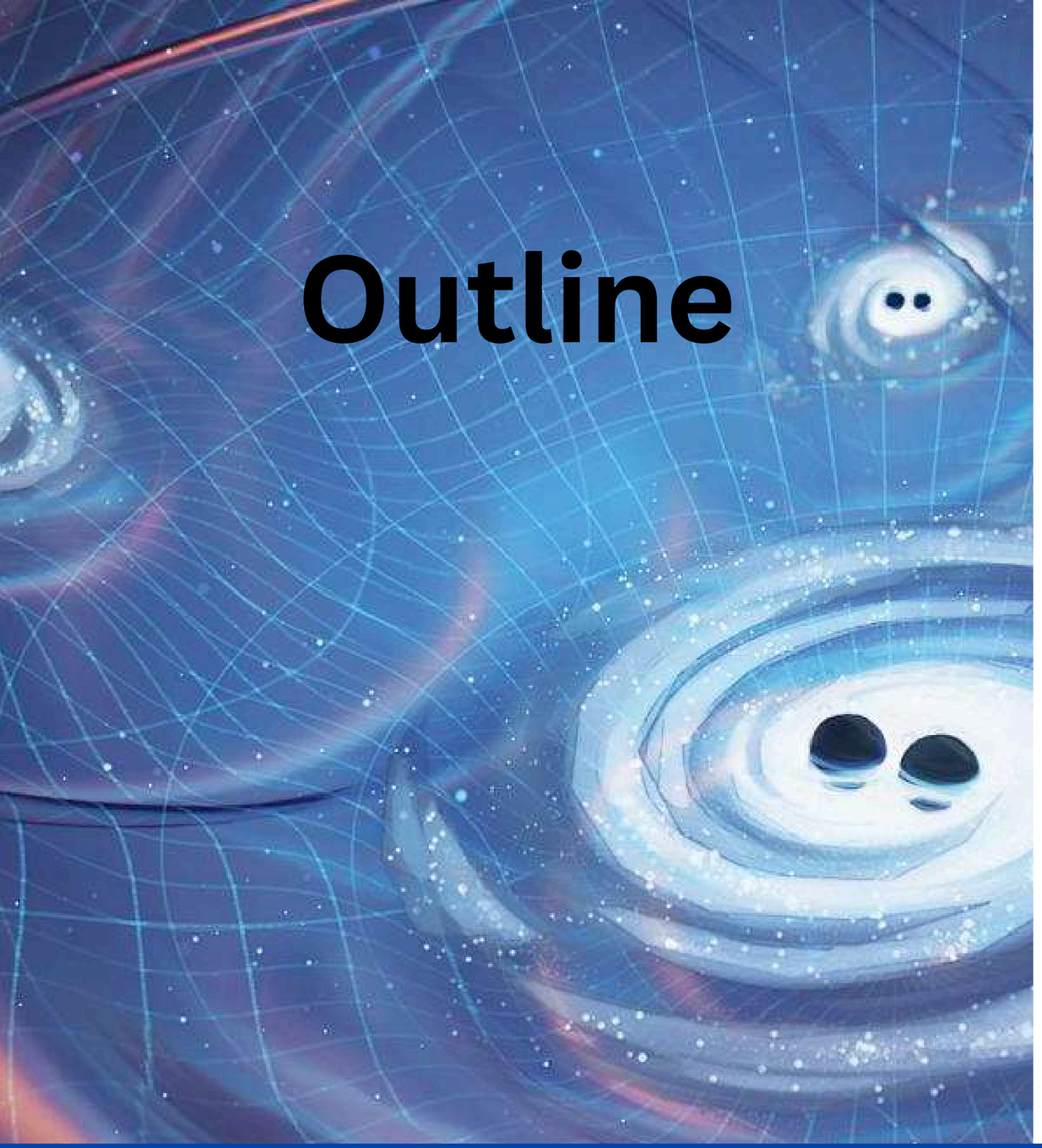
Presented By

Dr. Alba Romero-Rodríguez

Spontaneous Workshop XVIII

September 13rd – 19th, 2026, IESC Cargese, France

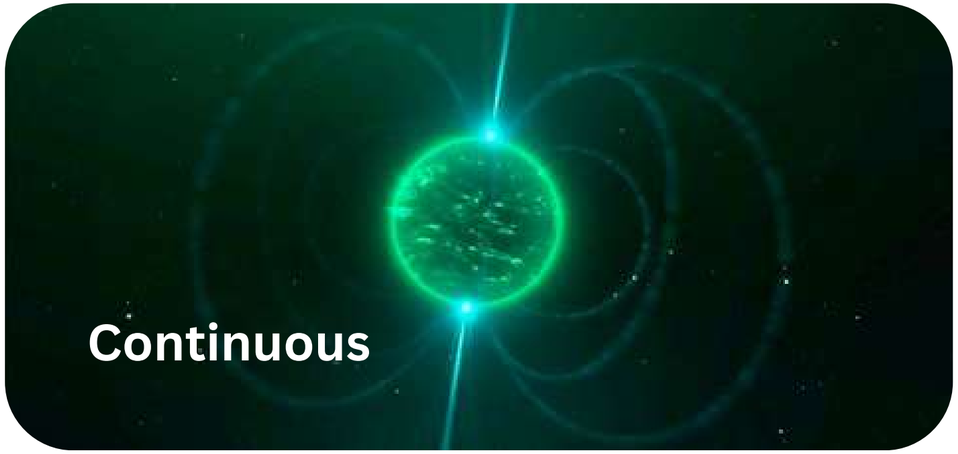
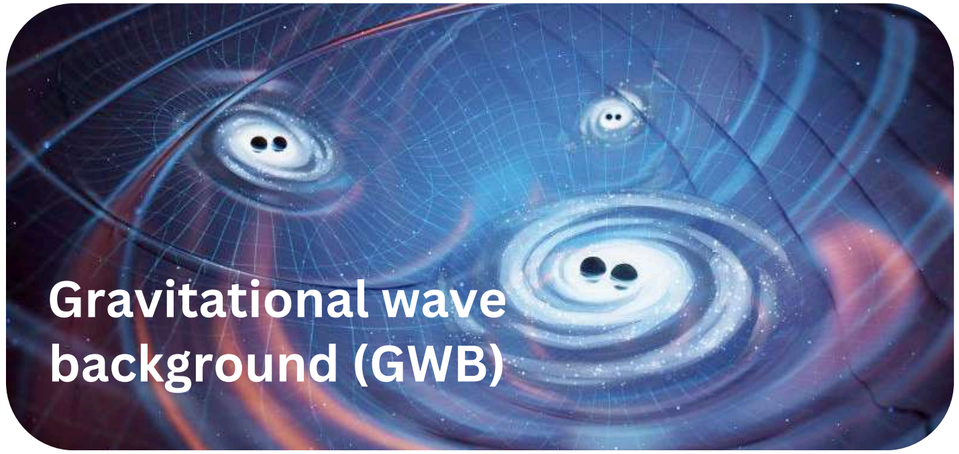




Outline

1. Sources of gravitational waves
2. Updates on GWTC-5
3. Gravitational wave background (GWB)
4. LVK search for an isotropic GWB
5. Current LVK results on the search for an isotropic GWB
6. Conclusions

Sources of GWs

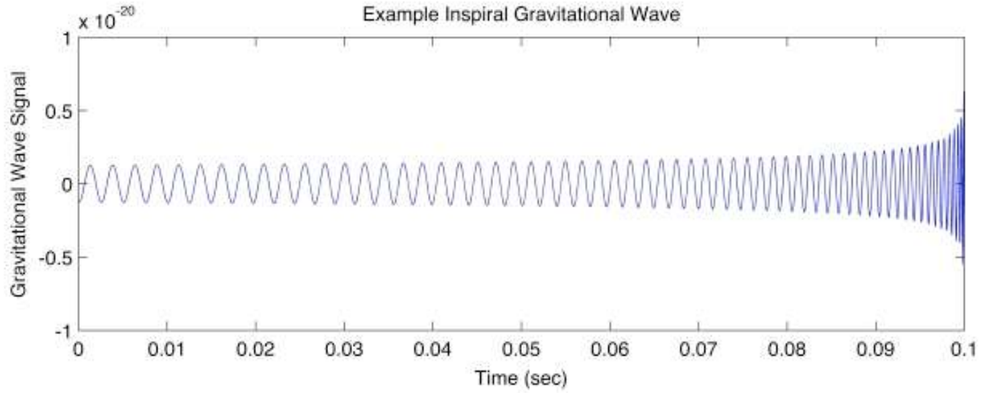
	Modelled	Unmodelled
Short duration		
Long duration		

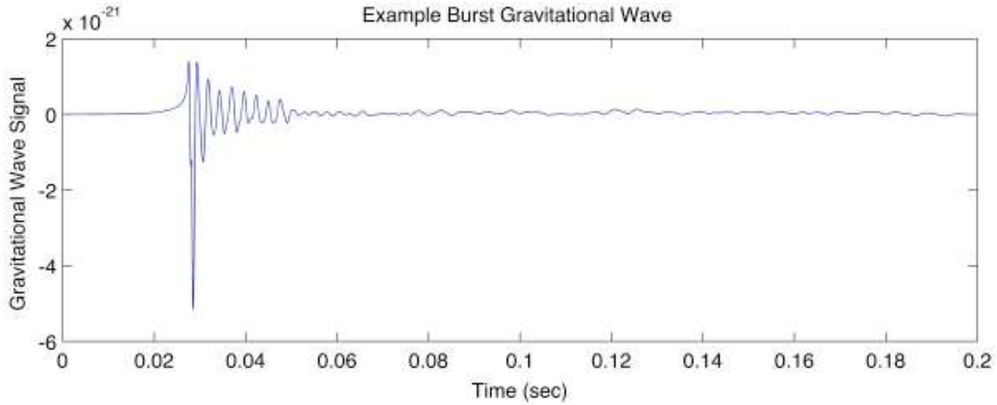
Sources of GWs

Modelled

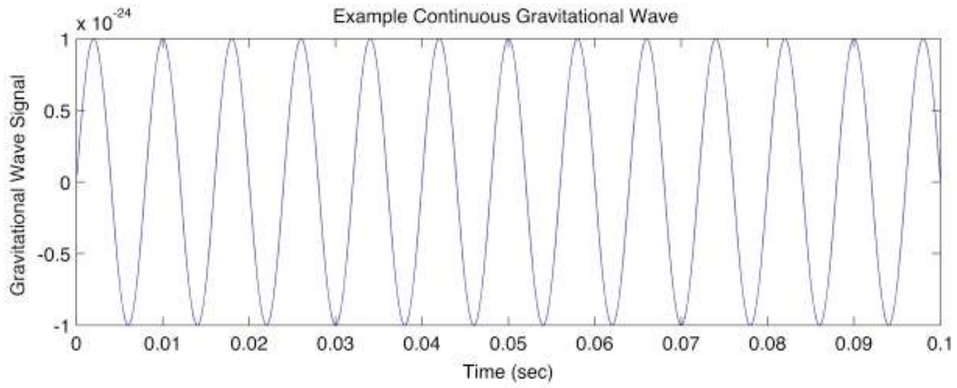
Unmodelled

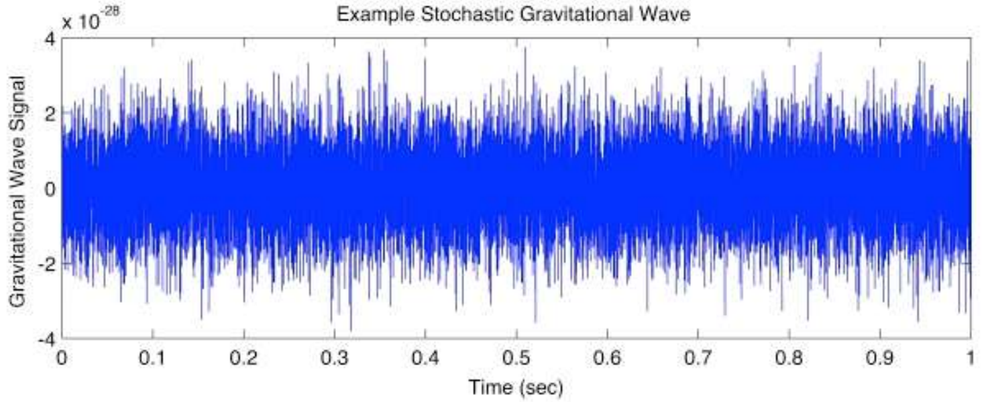
Short duration





Long duration



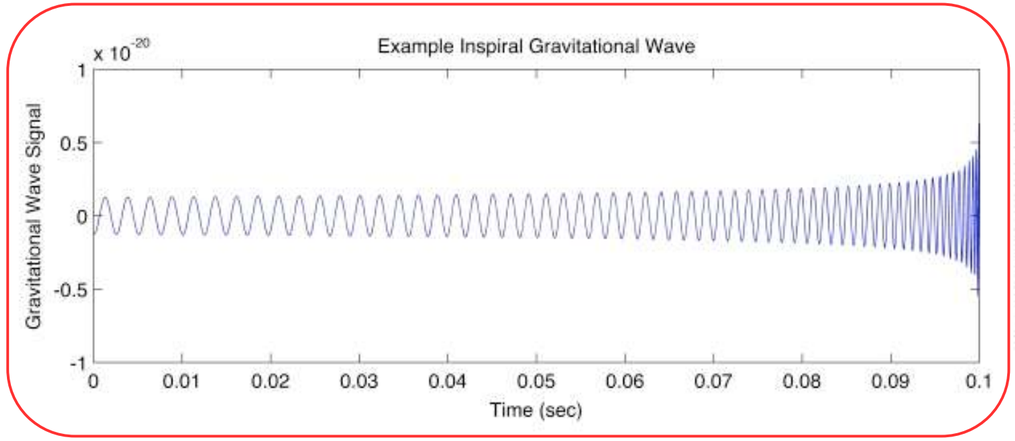


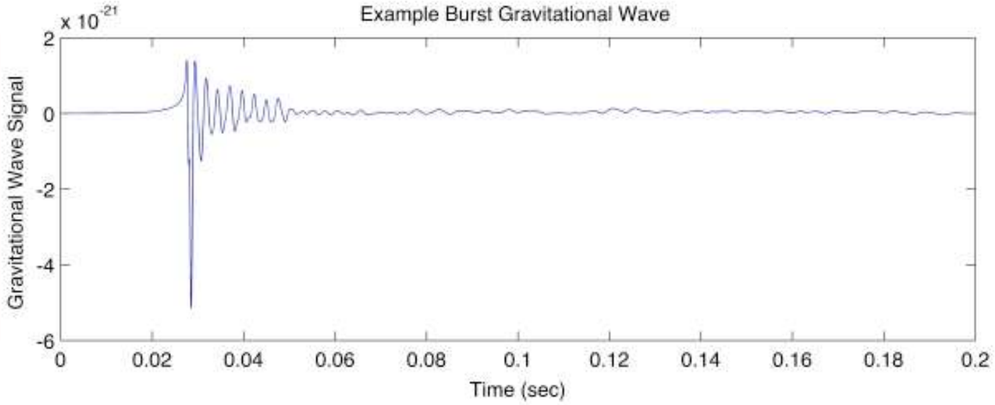
Sources of GWs

Modelled

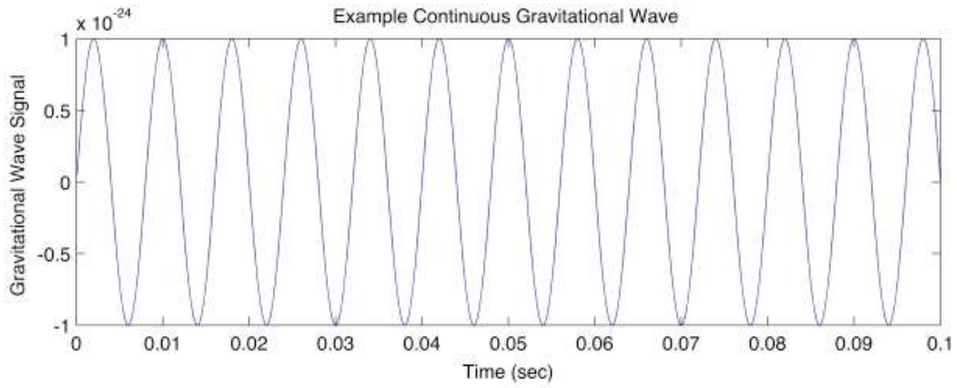
Unmodelled

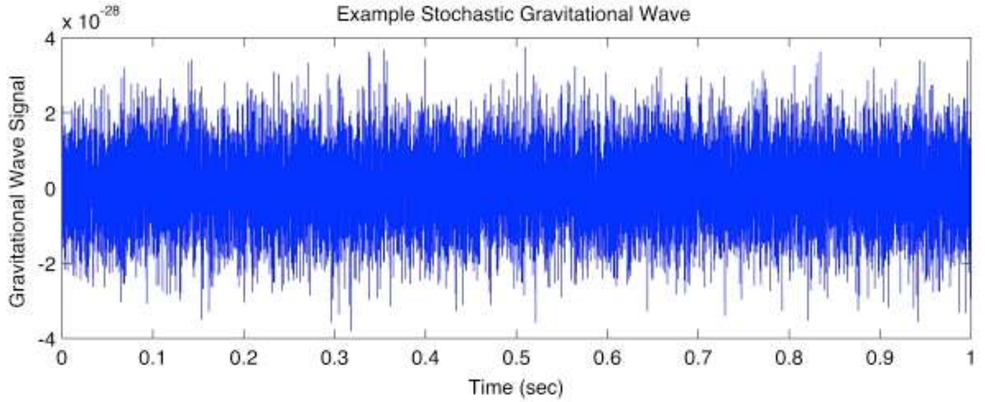
Short duration





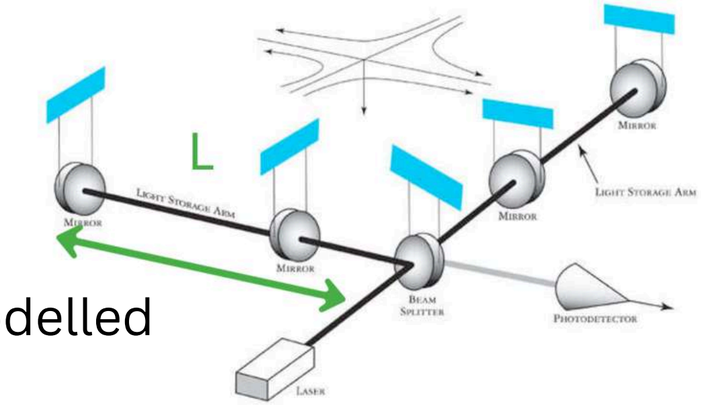
Long duration





Sources of GWs

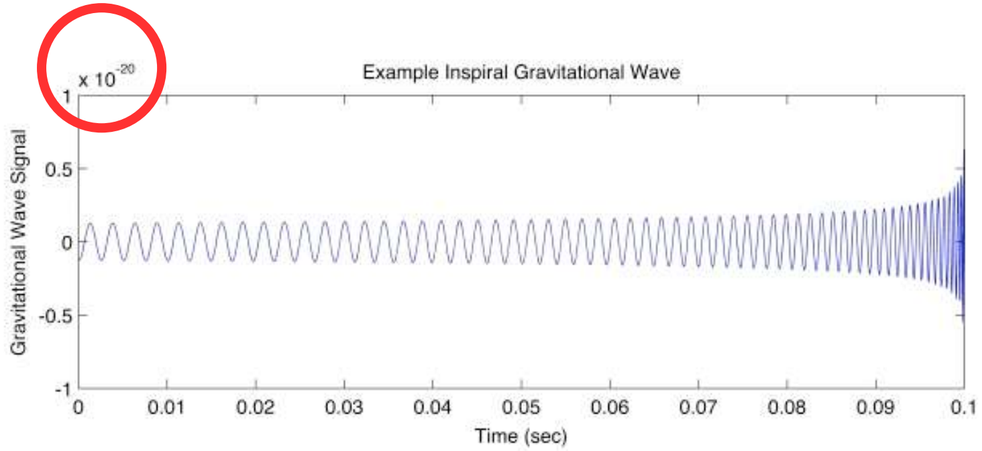
$$h = \frac{\Delta L}{L}$$

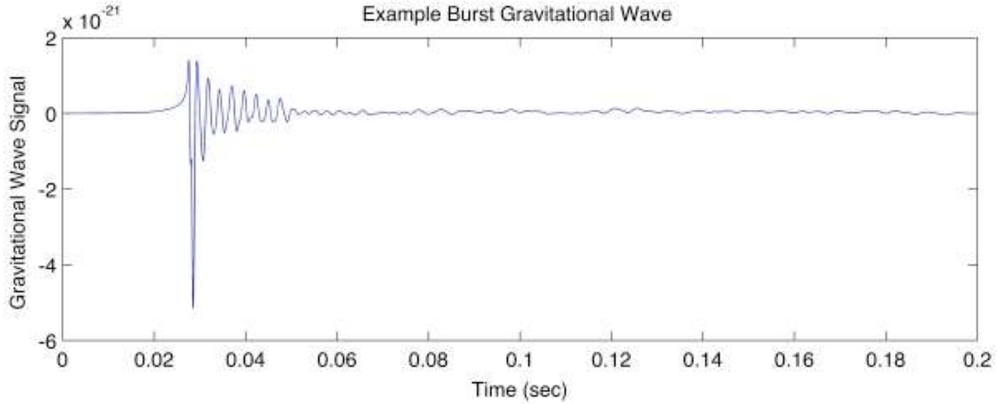


Modelled

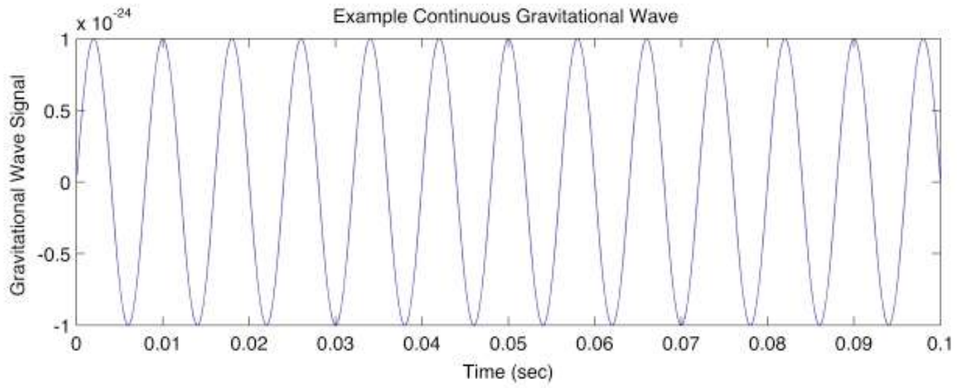
Unmodelled

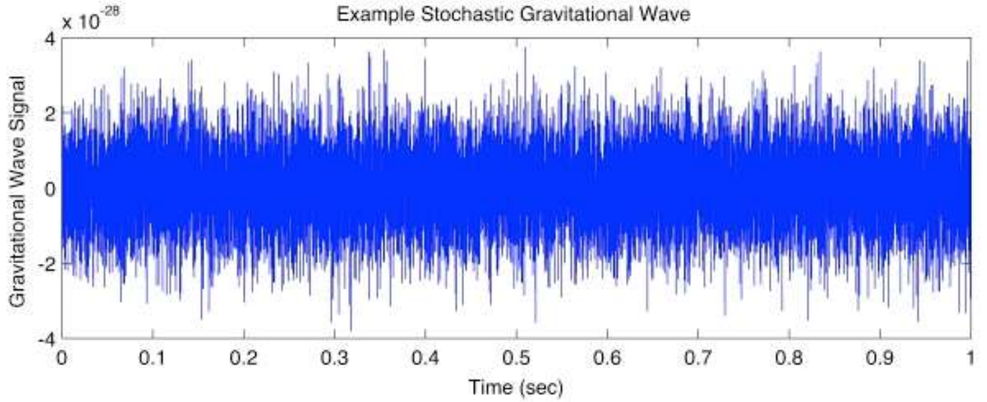
Short duration





Long duration



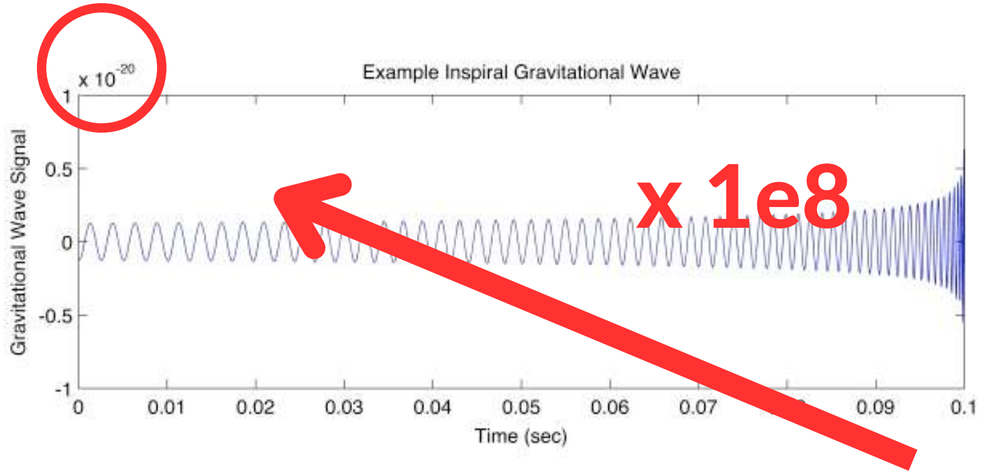


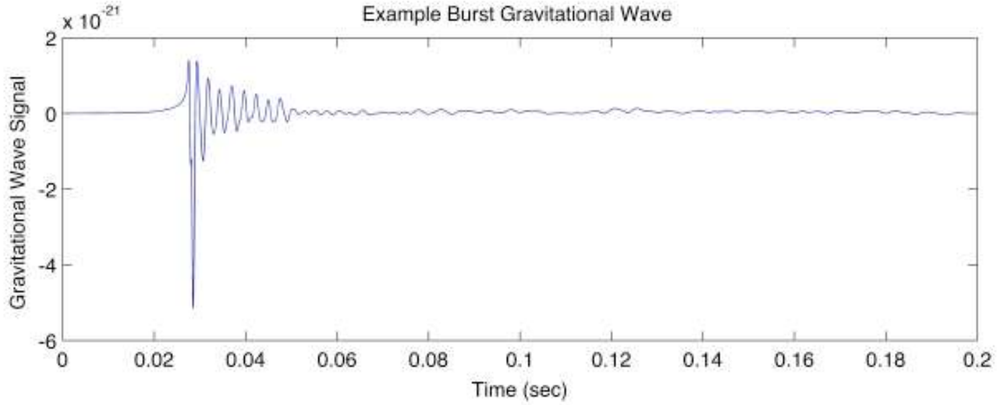
Sources of GWs

Modelled

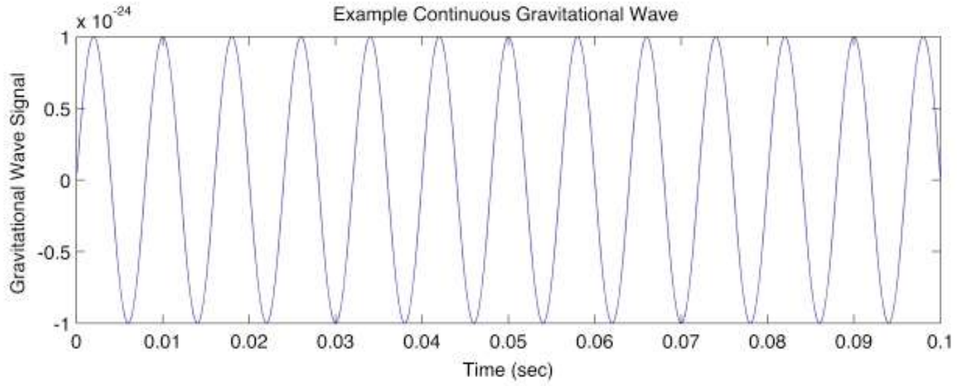
Unmodelled

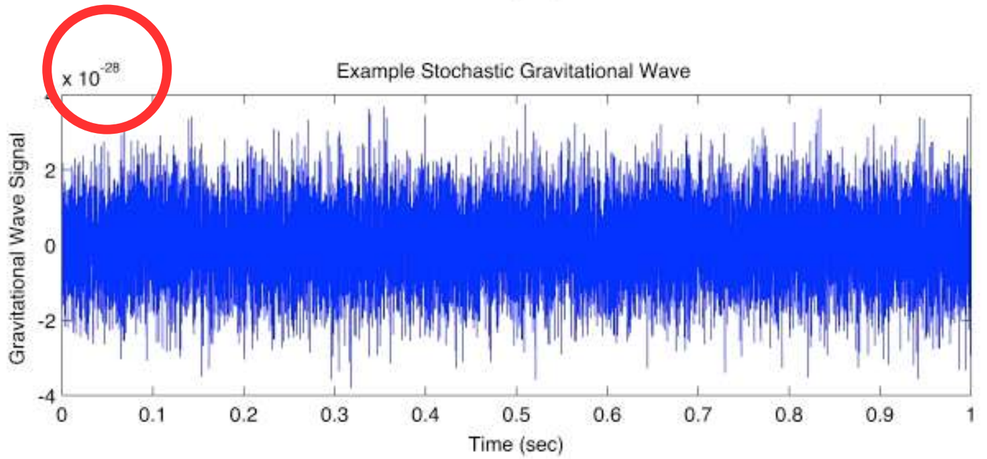
Short duration





Long duration



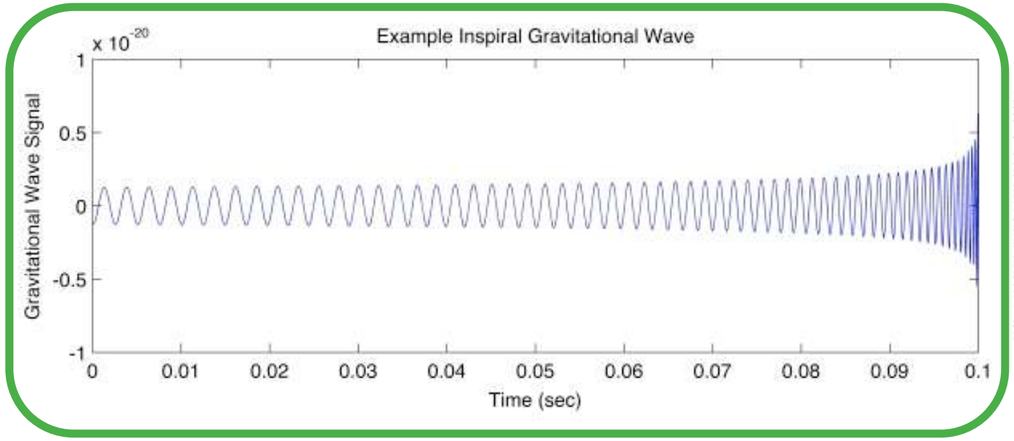


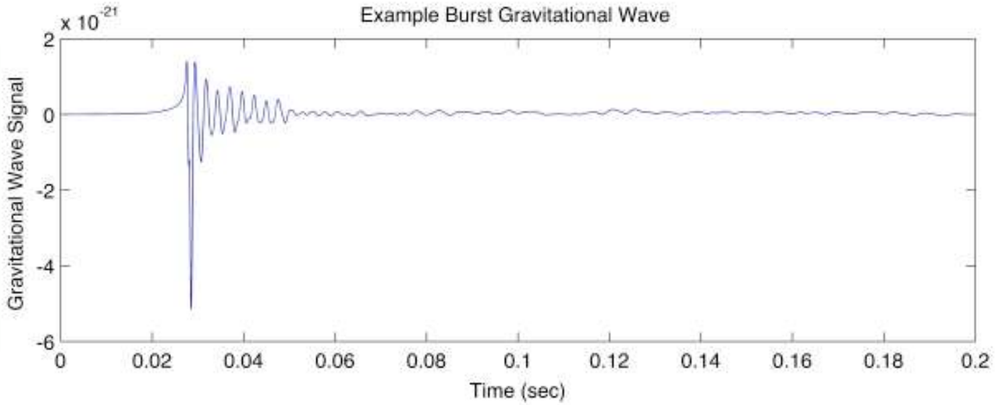
Sources of GWs

Modelled

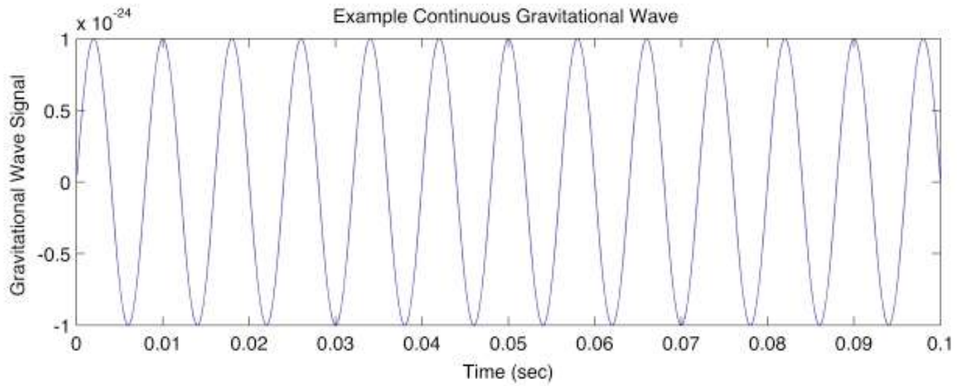
Unmodelled

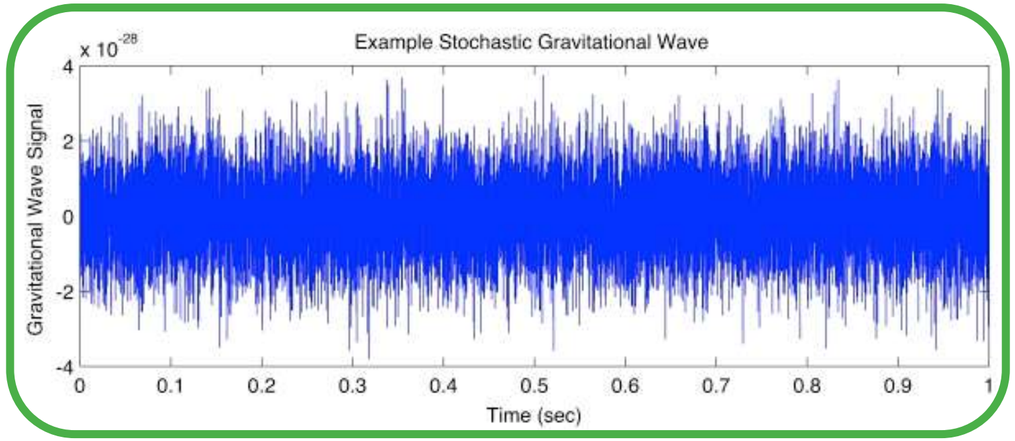
Short duration



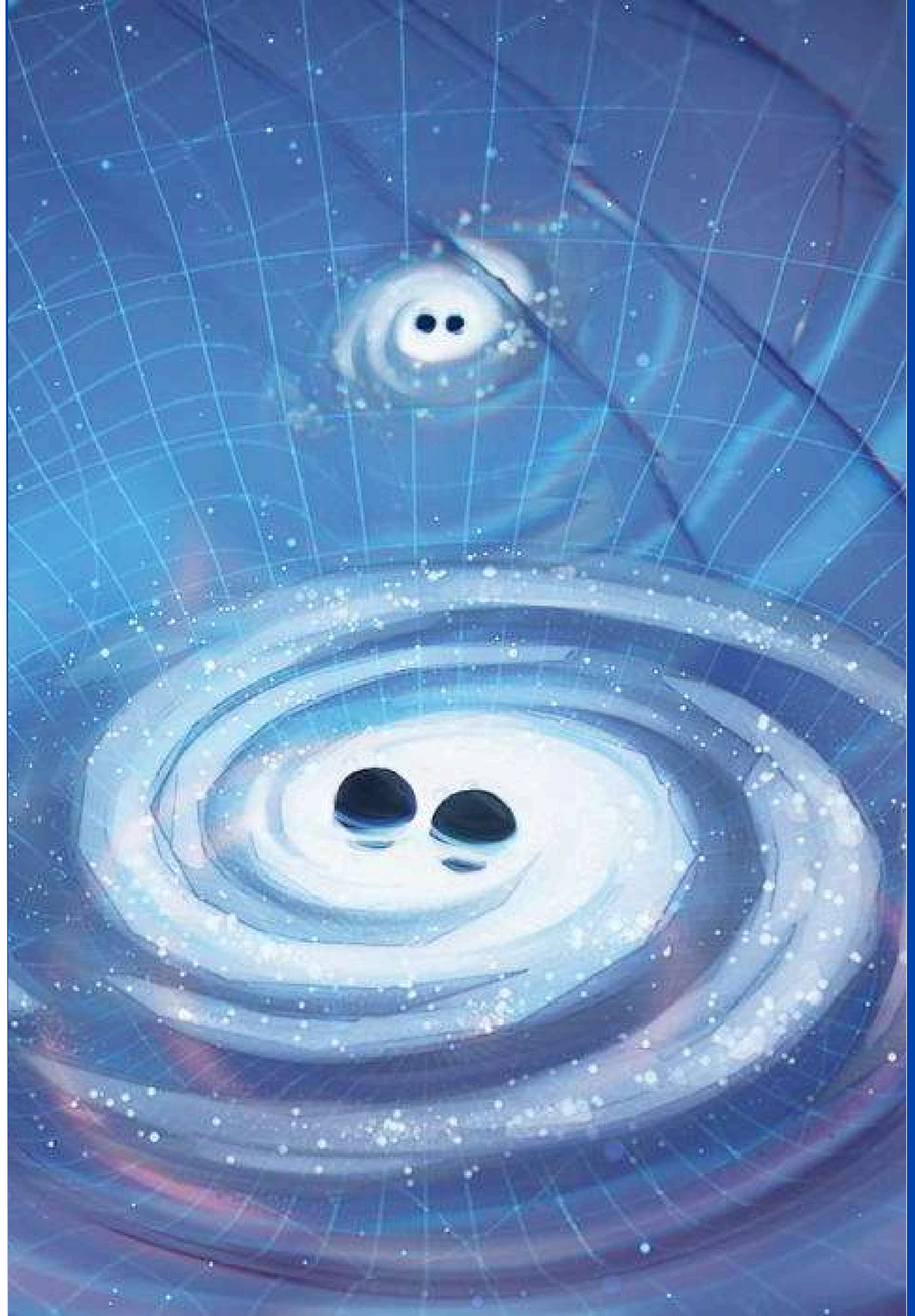


Long duration





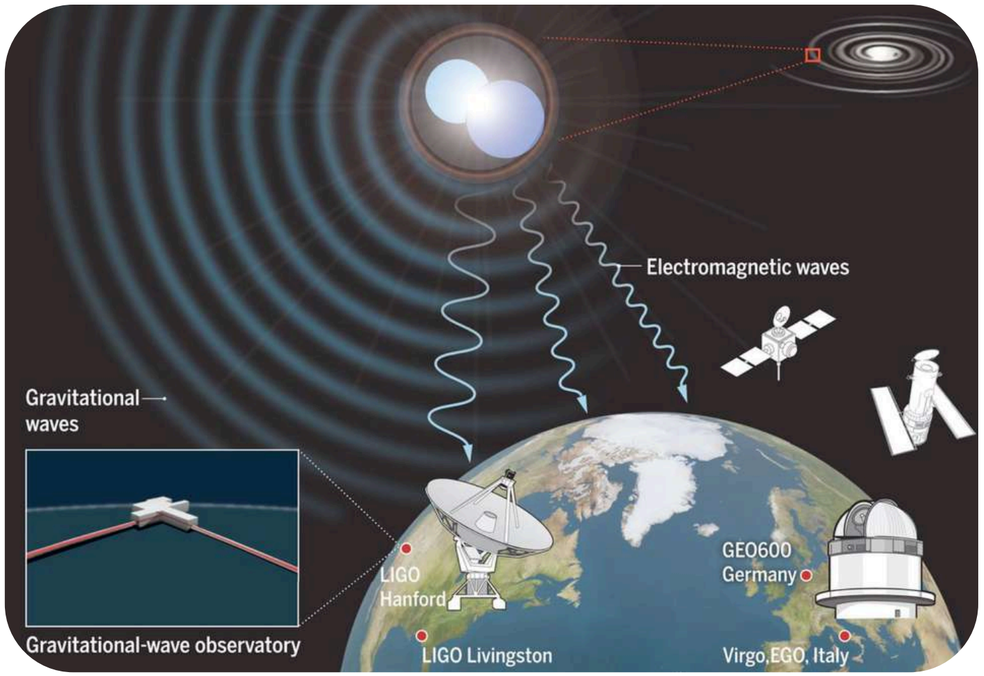
Updates from the fifth release of the Gravitational Wave Transient Catalog (GWTC-5)

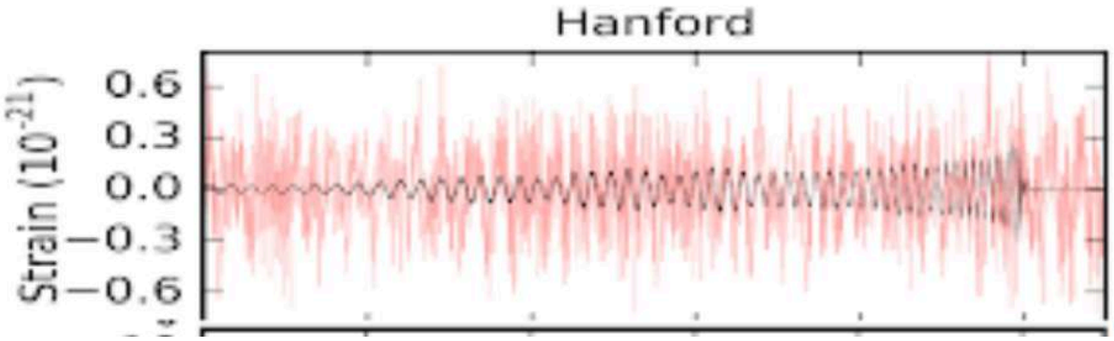


GWTC-5: Methods

- Search is carried out in 2 stages:
  - Online analyses → EM follow-up
  - Offline analyses → more accuracy
- Two types of detection algorithms:
  - Pipelines not relying on waveforms
  - Pipelines relying on waveforms: matched filtering

$$\rho(t) = 4 \left| \int_{f_{\text{low}}}^{f_{\text{high}}} \frac{h(f) u^*(f|\boldsymbol{\theta}_{\text{int}})}{S_n(f)} e^{2i\pi f t} df \right|$$

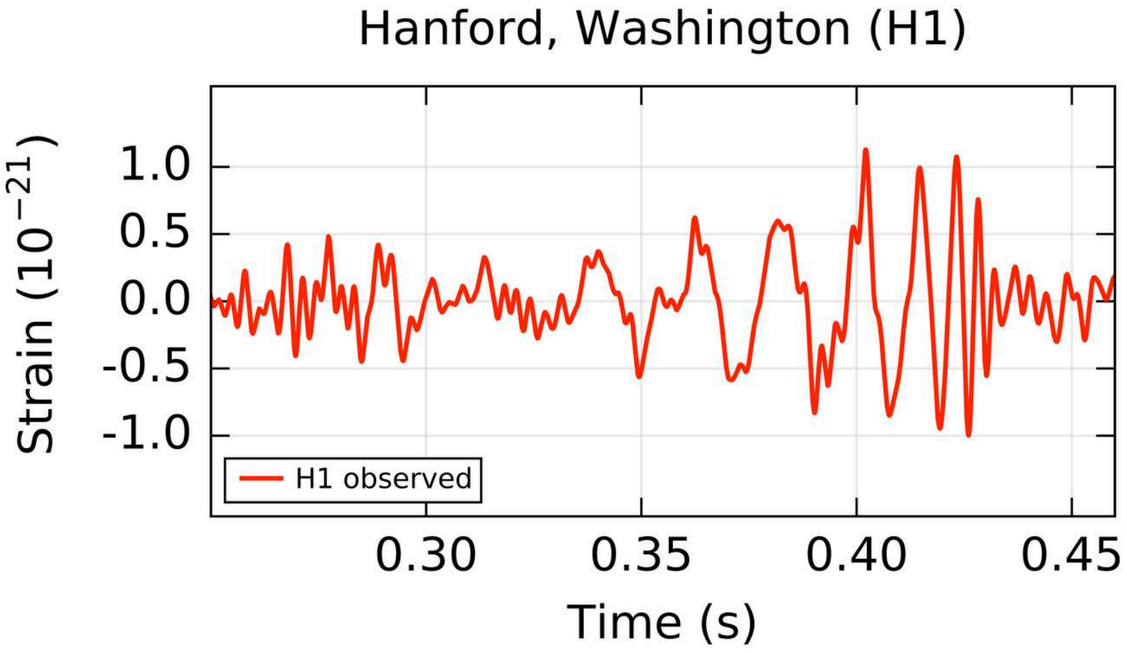




GWTC-5: Methods

- Search is carried out in 2 stages:
  - Online analyses → EM follow-up
  - Offline analyses → more accuracy
- Two types of detection algorithms:
  - Pipelines not relying on waveforms
  - Pipelines relying on waveforms: matched filtering

$$\rho(t) = 4 \left| \int_{f_{\text{low}}}^{f_{\text{high}}} \frac{h(f) u^*(f|\boldsymbol{\theta}_{\text{int}})}{S_n(f)} e^{2i\pi f t} df \right|$$

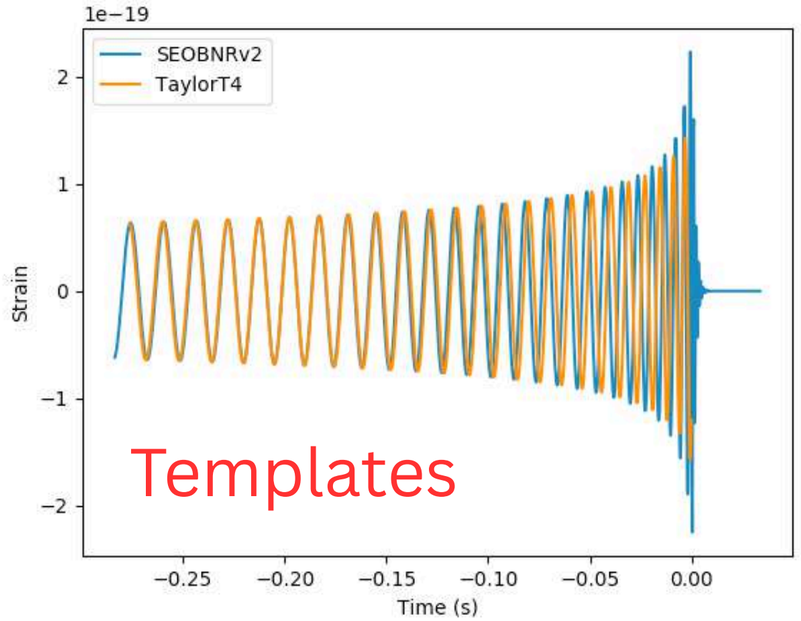


Strain data

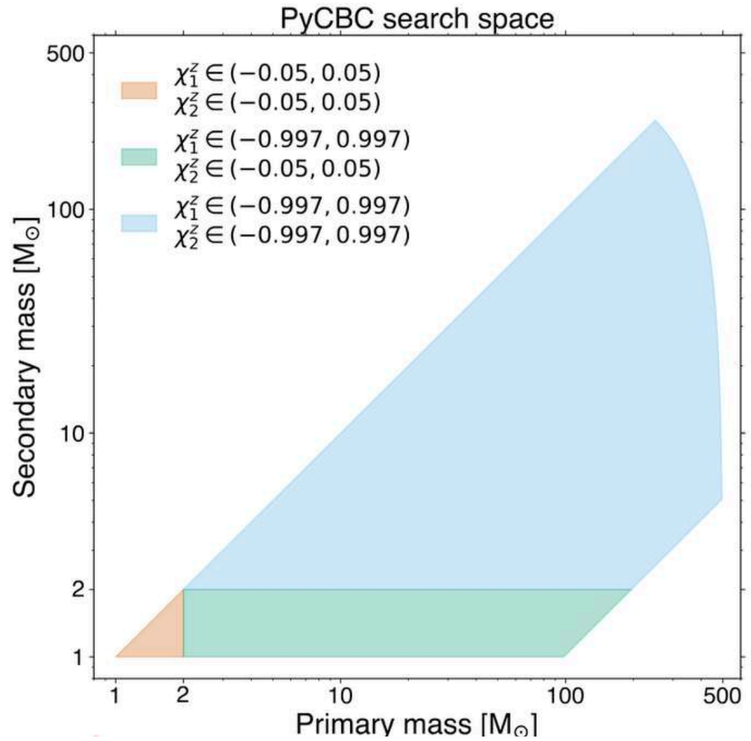
GWTC-5: Methods

- Search is carried out in 2 stages:
  - Online analyses → EM follow-up
  - Offline analyses → more accuracy
- Two types of detection algorithms:
  - Pipelines not relying on waveforms
  - Pipelines relying on waveforms: matched filtering

$$\rho(t) = 4 \left| \int_{f_{\text{low}}}^{f_{\text{high}}} \frac{h(f) u^*(f|\boldsymbol{\theta}_{\text{int}})}{S_n(f)} e^{2i\pi f t} df \right|$$



Template bank

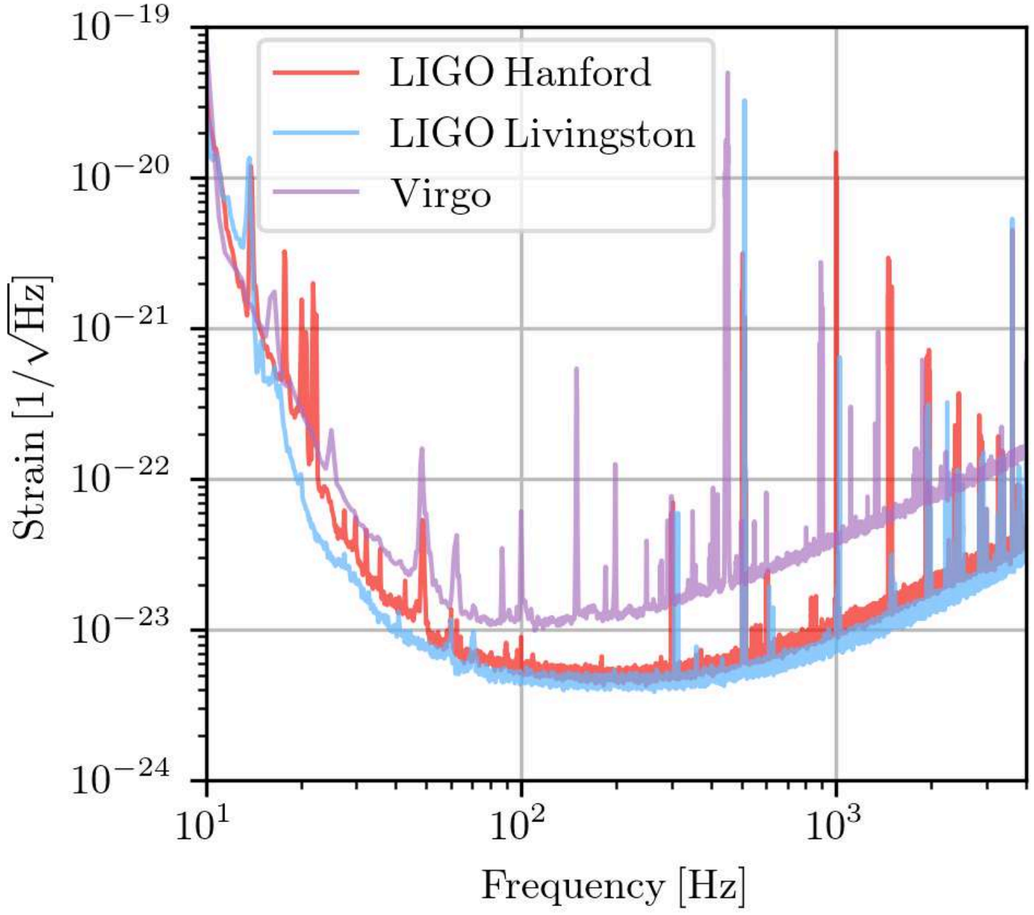


LVK Collaboration, arXiv:2508.18081 (2025)

GWTC-5: Methods

- Search is carried out in 2 stages:
  - Online analyses → EM follow-up
  - Offline analyses → more accuracy
- Two types of detection algorithms:
  - Pipelines not relying on waveforms
  - Pipelines relying on waveforms: matched filtering

$$\rho(t) = 4 \left| \int_{f_{\text{low}}}^{f_{\text{high}}} \frac{h(f) u^*(f|\boldsymbol{\theta}_{\text{int}})}{S_n(f)} e^{2i\pi f t} df \right|$$

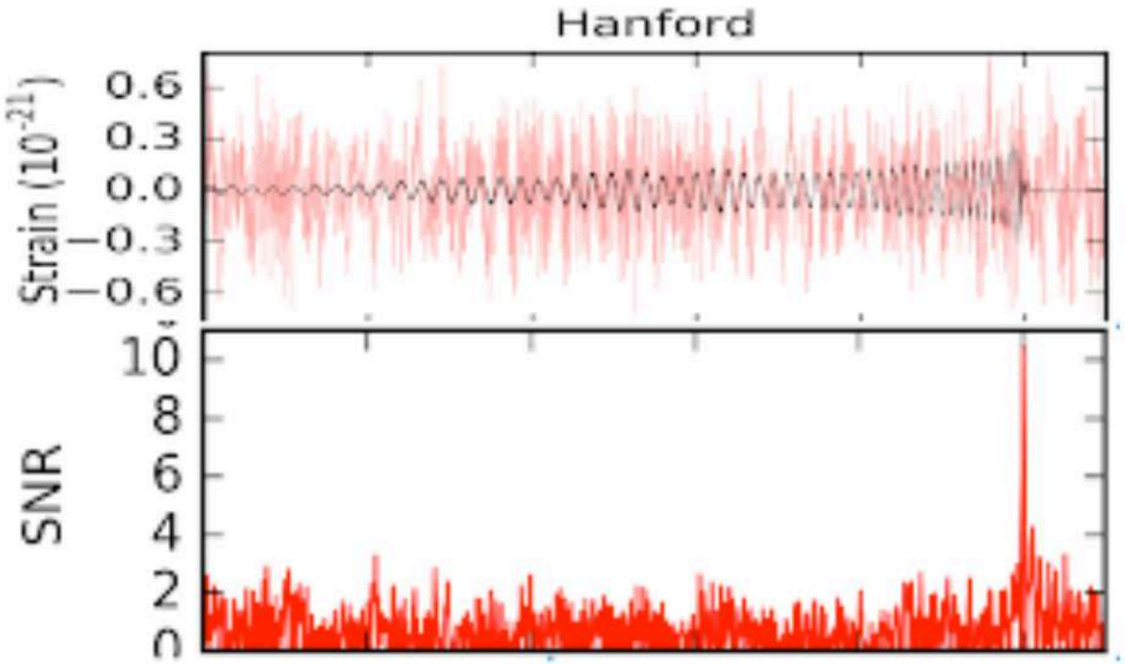


PSD of detector noise

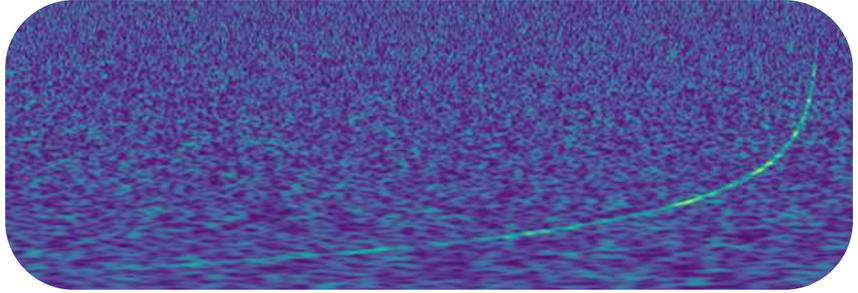
GWTC-5: Methods

- Search is carried out in 2 stages:
  - Online analyses → EM follow-up
  - Offline analyses → more accuracy
- Two types of detection algorithms:
  - Pipelines not relying on waveforms
  - Pipelines relying on waveforms: matched filtering

$$\rho(t) = 4 \left| \int_{f_{\rm low}}^{f_{\rm high}} \frac{h(f) u^*(f|\boldsymbol{\theta}_{\rm int})}{S_n(f)} e^{2i\pi f t} df \right|$$

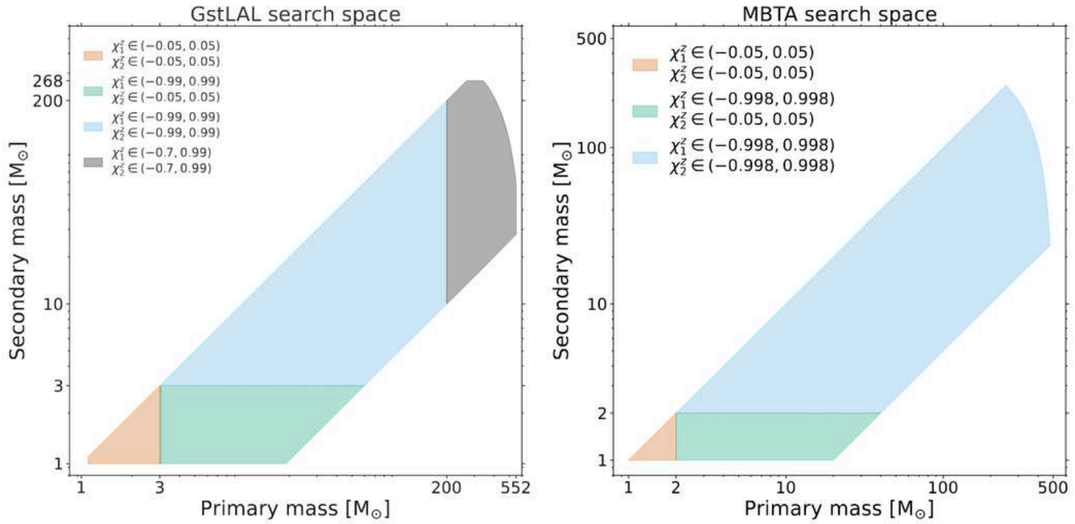


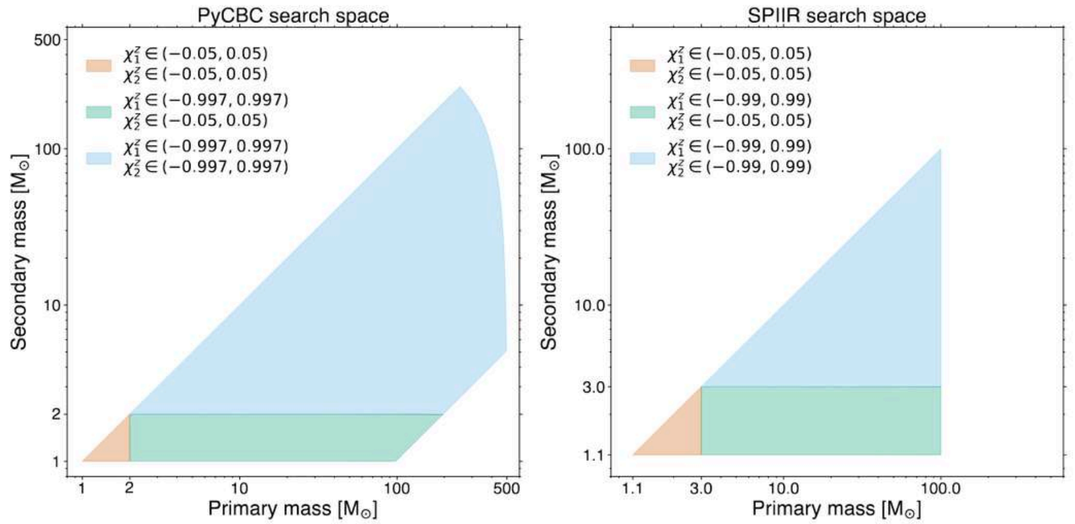
GWTC-5: Methods



Pipelines

- Coherent WaveBurst (cWB): minimally modelled sources → coincident excess power events
- GStreamer LIGO Algorithm Library (GstLAL): time-domain matched filtering
- Multi-Band Template Analysis (MBTA): matched filtering
- PyCBC: matched filtering
- Summed Paralell Infinite Impulse Response (SPIIR): time-domain matched filtering

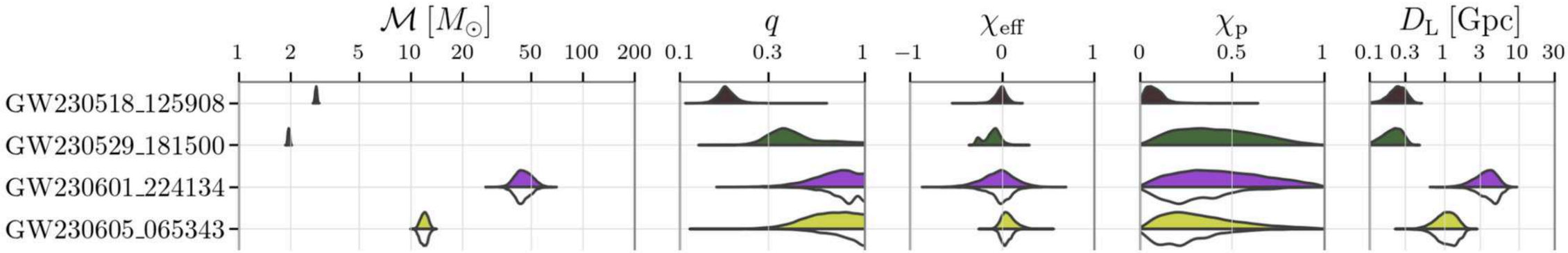




GWTC-5: Methods

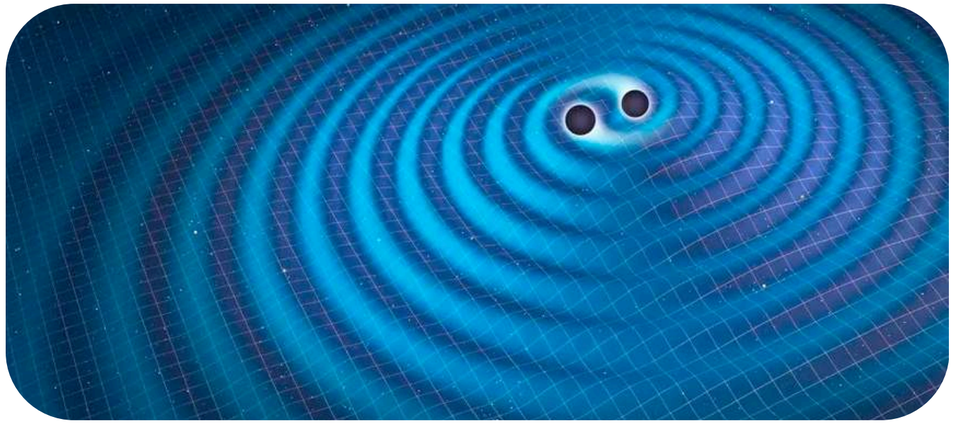
LVK Collaboration, arXiv:2508.18081 (2025)

- Each pipeline assigns each candidate:
  - FAR: expected rate of non-astrophysical candidates produced with a rank (ranking statistics) at least as high as the candidate under consideration
  - p_astro: probability that a candidate is of astrophysical origin rather than of terrestrial (noise)
- Bayesian inference is performed on a 15D parameter space



GWTC-5: Catalog updates

- O4b duration: 10/04/2024 - 28/01/2025
- Number of CBC candidates in O4b (detected by at least 1 pipeline): 161
  - No BNS nor NSBHs detected during O4b
- No confident multimenssenger counterpart
- Total number of candidates in full catalog: 390 with p_astro >= 0.5
- Candidates with FAR < 1/ year and p_astro >= 0.5 are of high-purity





GWTC-5: Catalog updates

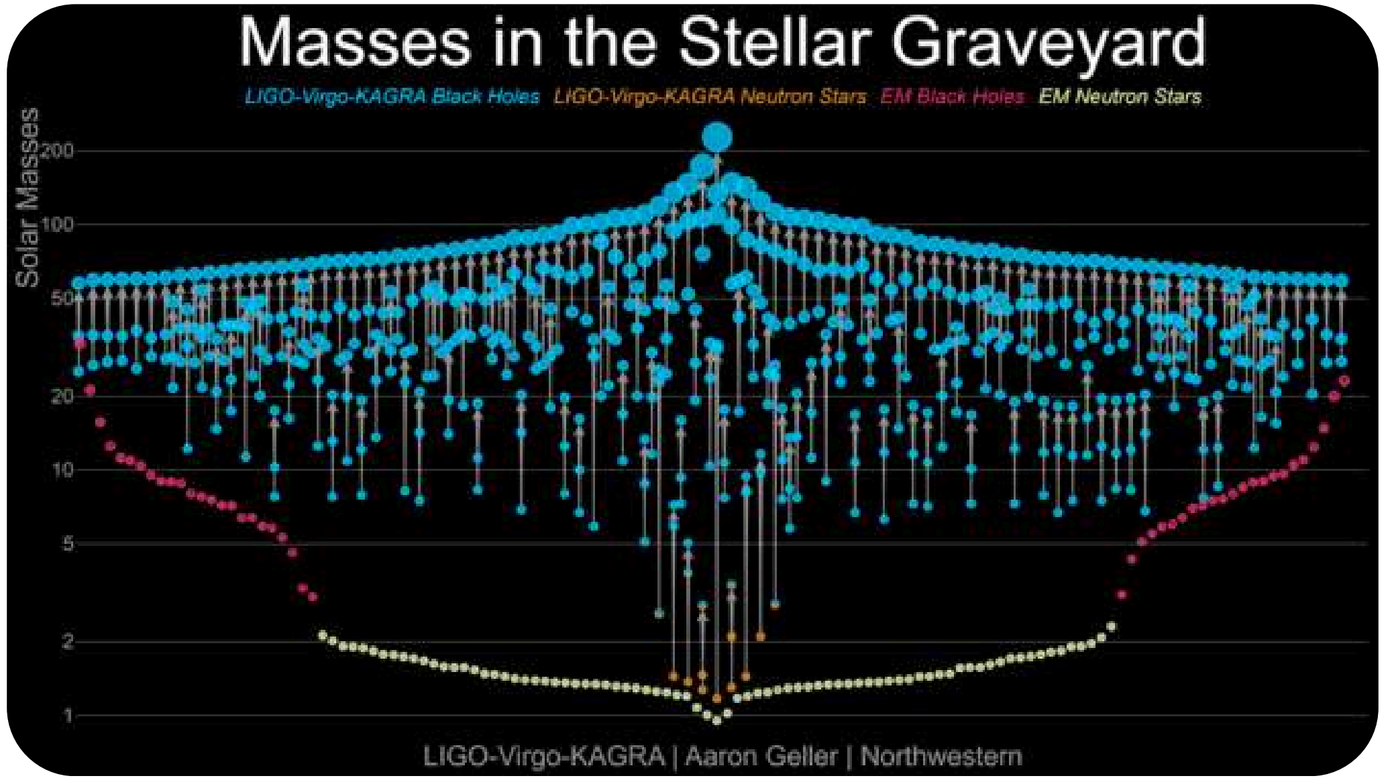
- Interesting findings during O4b:
  - Some signals detected with SNR > 30. The one with highest SNR (= 76.9): GW250114_082203
  - Event with most precise sky localization (6 deg^2 at 90% CL): GW240615_113620
- Most massive signal is still one from O4a : GW231123_135430 (source frame total mass: $236^{+29}_{-48}\,M_\odot$)

Candidate	M $[M_\odot]$	$\mathcal{M}$ $[M_\odot]$	m_1 $[M_\odot]$	m_2 $[M_\odot]$	χ_{eff}	D_{L} [Gpc]	z	M_{f} $[M_\odot]$	χ_{f}	$\Delta\Omega$ $[\mathrm{deg}^2]$	SNR
GW231119_075248	$82^{}_{-18}$	$34.4^{}_{-7.8}$	$49^{}_{-13}$	$34^{}_{-13}$	$-0.002^{}_{-0.302}$	$6.7^{}_{-3.7}$	$0.99^{}_{-0.48}$	$79^{}_{-18}$	$0.68^{}_{-0.16}$	5900	$7.7^{}_{-0.5}$
GW231123_135430	236^{+29}_{-48}	101^{+13}_{-30}	137^{+23}_{-18}	101^{+22}_{-51}	$0.3^{+0.2}_{-0.4}$	$2.2^{+2.0}_{-1.5}$	$0.39^{+0.28}_{-0.25}$	222^{+27}_{-42}	$0.84^{+0.07}_{-0.19}$	1700	$20.7^{+0.2}_{-0.3}$
GW231127_165300	74^{+22}_{-}	$30.5^{+9.5}_{-}$	45^{+18}_{-}	29^{+12}_{-}	$0.05^{+0.30}_{-}$	$4.5^{+3.6}_{-}$	$0.71^{+0.44}_{-}$	71^{+21}_{-}	$0.69^{+0.12}_{-}$	4400	$8.3^{+0.3}_{-}$
GW250109_074332	$69.2^{}_{-8.6}$	$29.0^{}_{-3.8}$	$39.0^{}_{-6.3}$	$30.2^{}_{-7.2}$	$0.07^{}_{-0.20}$	$2.3^{}_{-1.1}$	$0.41^{}_{-0.18}$	$65.9^{}_{-8.1}$	$0.72^{}_{-0.09}$	7500	$10.9^{}_{-0.5}$
GW250114_082203	$66.0^{+1.1}_{-1.2}$	$28.71^{+0.50}_{-0.51}$	$33.76^{+1.28}_{-0.90}$	$32.26^{+0.95}_{-1.47}$	$-0.03^{+0.04}_{-0.05}$	$0.40^{+0.08}_{-0.07}$	$0.09^{+0.02}_{-0.01}$	$62.9^{+1.0}_{-1.1}$	$0.68^{+0.01}_{-0.01}$	42	$76.9^{+0.0}_{-0.1}$
GW250116_015318	56^{+16}_{-}	$23.0^{+6.9}_{-}$	$34.2^{+14.5}_{-}$	$21.3^{+8.8}_{-}$	$0.15^{+0.31}_{-}$	$5.2^{+3.9}_{-}$	$0.80^{+0.47}_{-}$	53^{+15}_{-}	$0.73^{+0.12}_{-}$	3000	$7.6^{+0.4}_{-}$
GW240612_081540	$92^{}_{-18}$	$38.5^{}_{-8.5}$	$55^{}_{-13}$	$38^{}_{-16}$	$0.07^{}_{-0.34}$	$6.2^{}_{-3.1}$	$0.95^{}_{-0.40}$	$88^{}_{-17}$	$0.71^{}_{-0.15}$	2800	$7.4^{}_{-0.6}$
GW240615_113620	$60.4^{+3.5}_{-2.5}$	$25.9^{+1.7}_{-1.2}$	$34.0^{+5.4}_{-3.7}$	$26.4^{+4.0}_{-4.8}$	$-0.07^{+0.11}_{-0.13}$	$1.56^{+0.29}_{-0.45}$	$0.29^{+0.05}_{-0.08}$	$57.8^{+3.3}_{-2.4}$	$0.66^{+0.05}_{-0.06}$	6	$23.8^{+0.1}_{-0.2}$
GW240615_160735	$48.5^{+8.5}_{-}$	$20.4^{+4.0}_{-}$	$28.5^{+7.9}_{-}$	$20.0^{+5.7}_{-}$	$0.28^{+0.20}_{-}$	$4.0^{+1.9}_{-}$	$0.65^{+0.24}_{-}$	$45.0^{+8.0}_{-}$	$0.78^{+0.08}_{-}$	1100	$9.9^{+0.3}_{-}$

LVK Collaboration, arXiv:2605.27225 (2026)

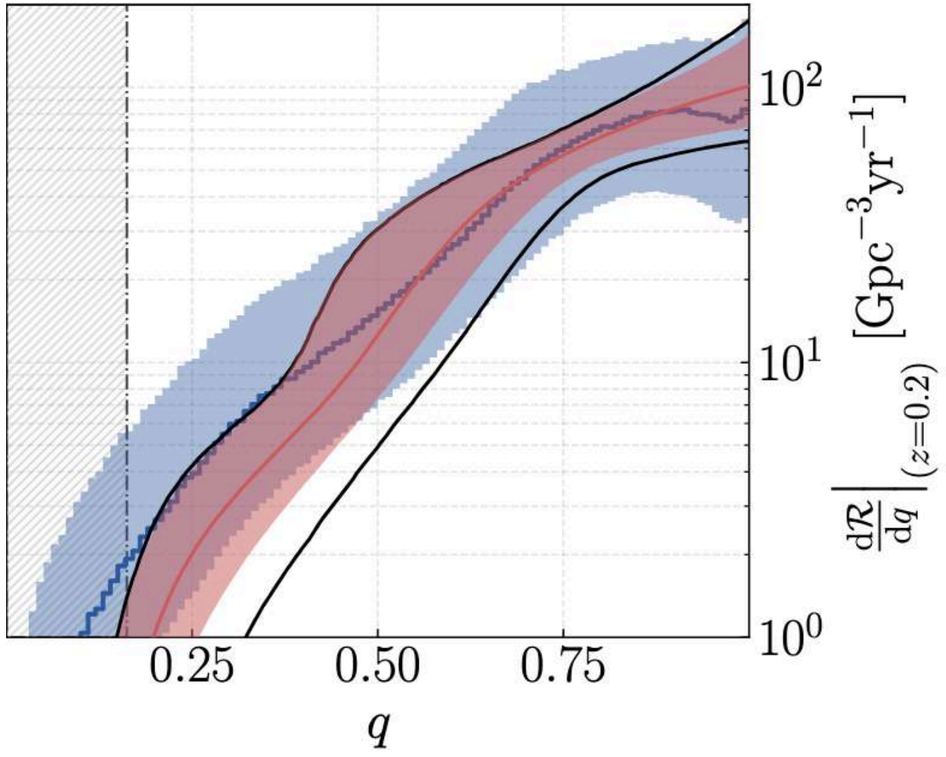
GWTC-5: CBC population updates

- To update the CBC pops properties: 267 CBC candidates have been used (FAR < 1 / year)
- Analysis supports presence of multiple BBH subpopulations → multiple formation mechanisms
- Analysis rules out a completely empty gap between 3-5 Msol



GWTC-5: BBH population properties - mass ratio

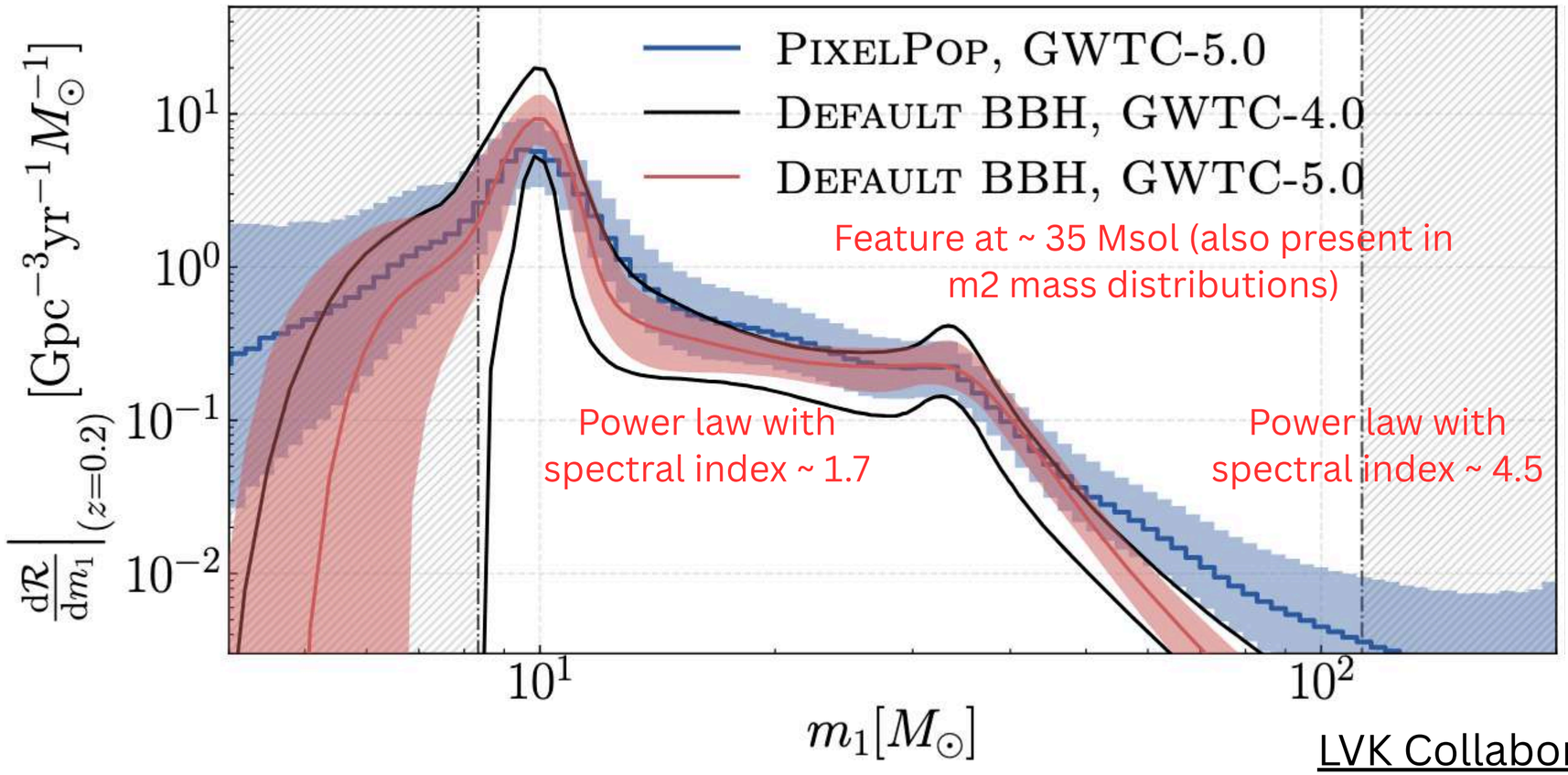
- The global BBH mass ratio distribution is consistent with a peak at q = 1
- BHs with masses ~ 35 Msol preferentially merge with BHs of = mass (favoured by most formation channels)
- BHs with masses ~ 10 Msol preferentially merge with lighter BHs



LVK Collaboration, arXiv:2605.27226 (2026)

GWTC-5: BBH population properties - mass distribution

Global peak at ~10 Msol (predicted by isolated binary evolution models)

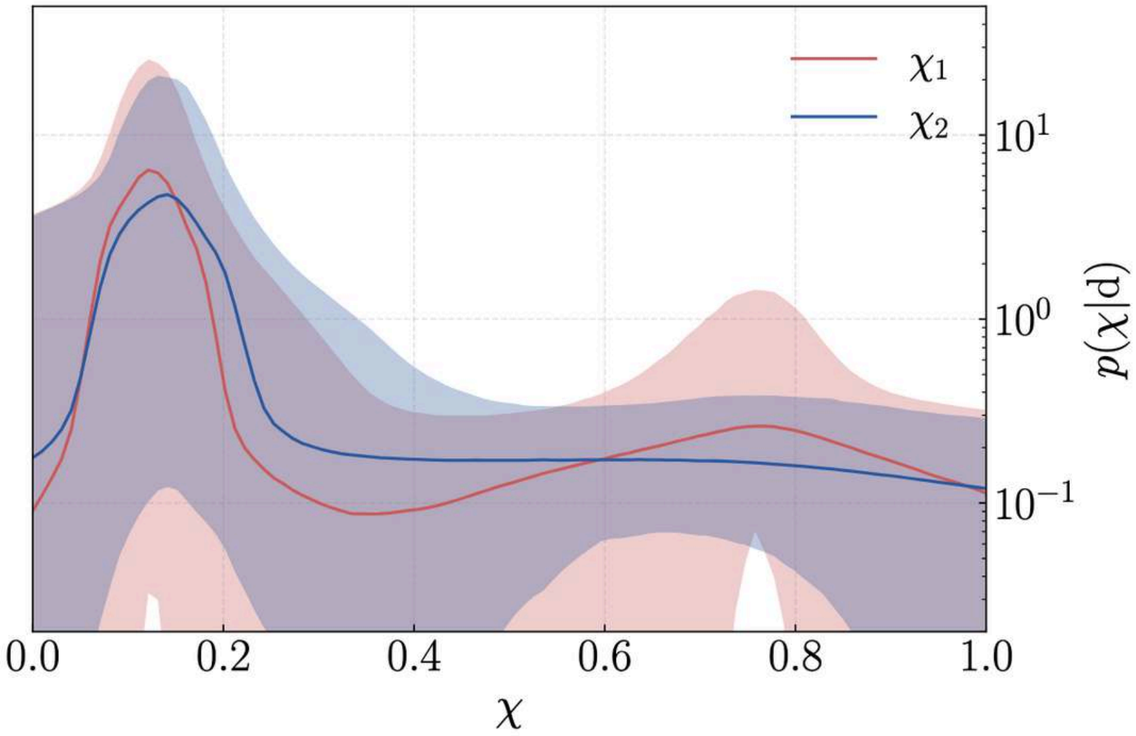


No hints of peaks around 20 and 60 Msol, as predicted with GWTC-4 data

LVK Collaboration, arXiv:2605.27226 (2026)

GWTC-5: BBH population properties - spin

- Most BHs have relatively small spins: about 69%–84% have spin magnitude $\chi \leq 0.5$ (depending on the population model)
- Evidence for a subpopulation with at least one rapidly spinning BH, with $\chi \sim 0.7$ (corresponding to masses around 10–20 $M_\odot$ and $m1 > 40 M_\odot$) → consistent with a possible hierarchical-merger contribution



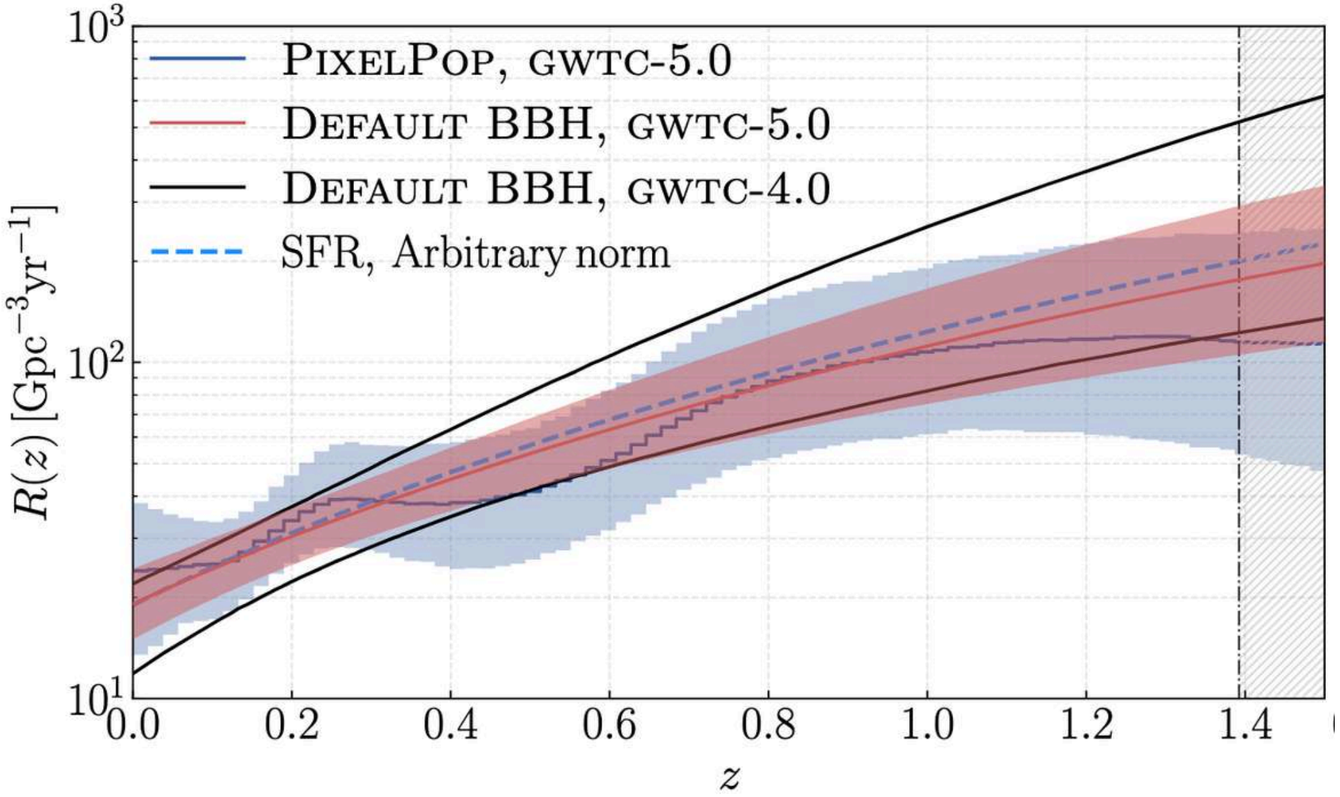
LVK Collaboration, arXiv:2605.27226 (2026)

GWTC-5: BBH population properties - merger rate

BBH merger rate at z = 0.2:

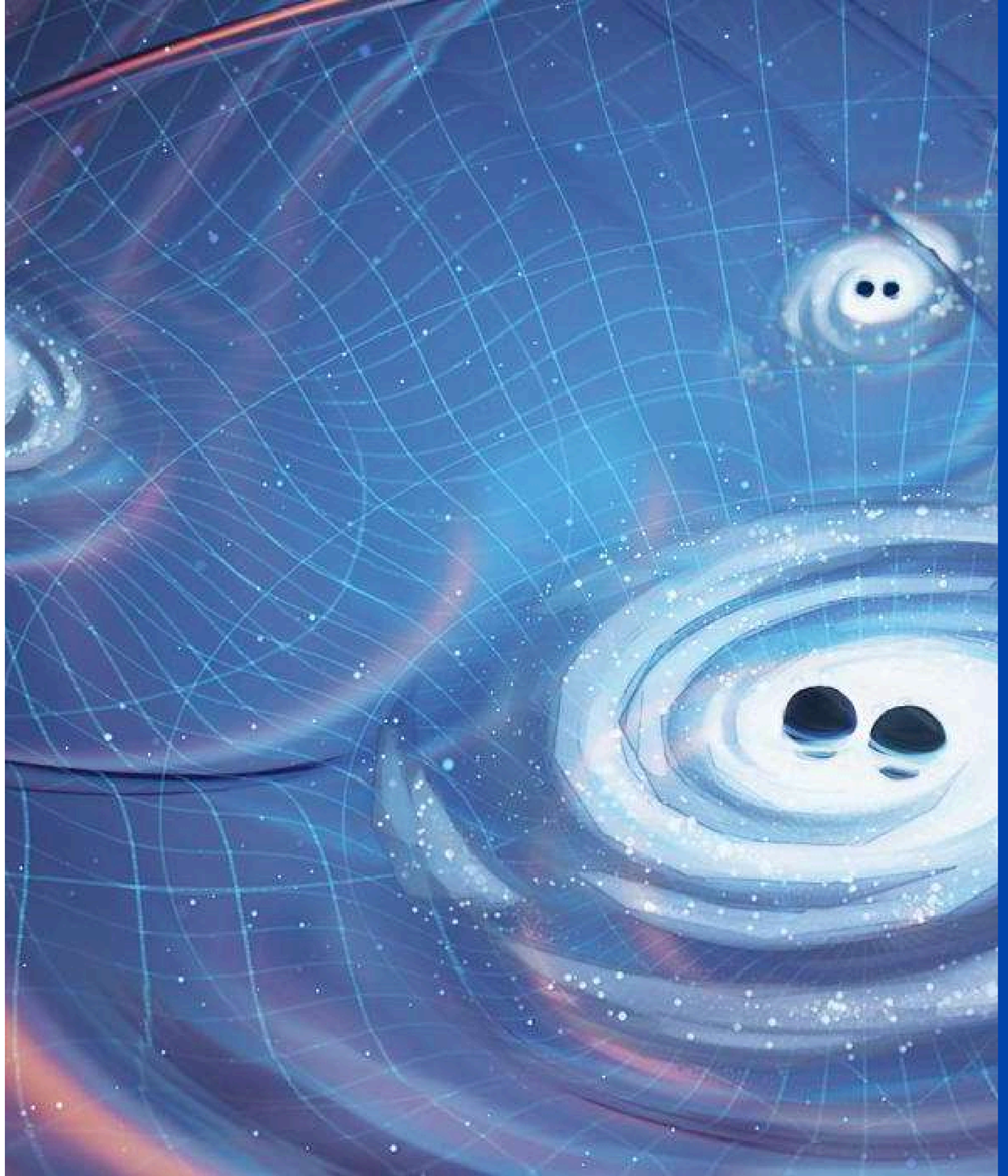
$$30.4^{+6.5}_{-5.4}\,(32.8^{+10.7}_{-7.6})\,\mathrm{Gpc}^{-3}\,\mathrm{yr}^{-1}$$

BBH merger-rate evolution consistent with the cosmic star-formation history



LVK Collaboration, arXiv:2605.27226 (2026)

O4 LVK results on the search for an isotropic GWB

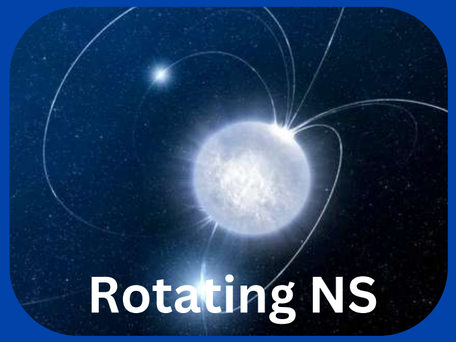


Gravitational wave background

Superposition of random GW signals produced by a large number of weak, independent and unresolved sources

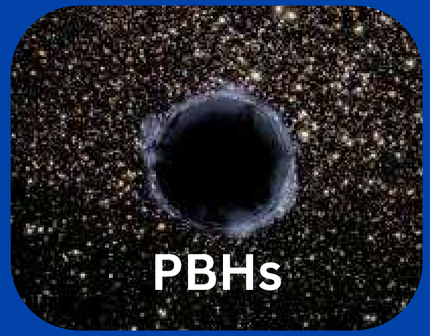












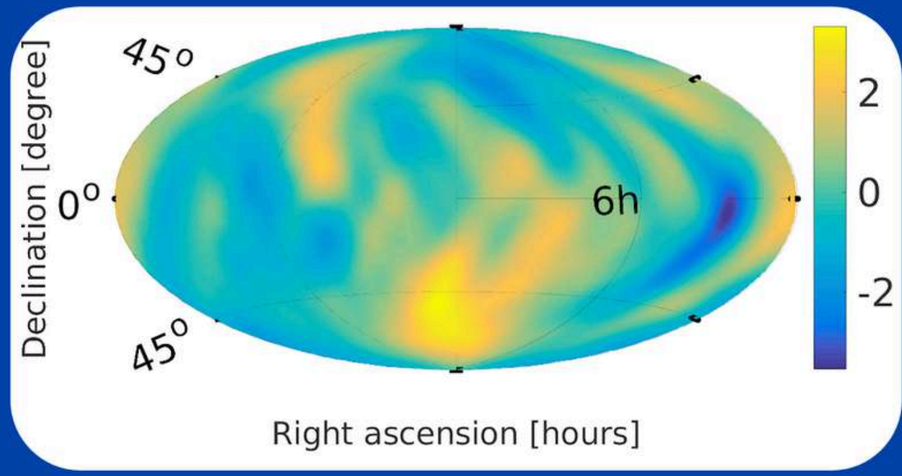
GWB characterization

- Statistically: probability distribution or moments
- Large number of independent sources: GWB is Gaussian

$$\langle h_{ab}(t,\vec{x})\rangle, \quad \langle h_{ab}(t,\vec{x})h_{cd}(t',\vec{x}')\rangle$$

Assumptions

- Isotropic
- Stationary
- Unpolarized
- Gaussian



$$\left\langle h_A(f,\hat{n})h^*_{A'}(f',\hat{n}')\right\rangle = \frac{1}{16\pi}S_h(f)\delta(f-f')\delta_{AA'}\delta^2(\hat{n},\hat{n}')$$

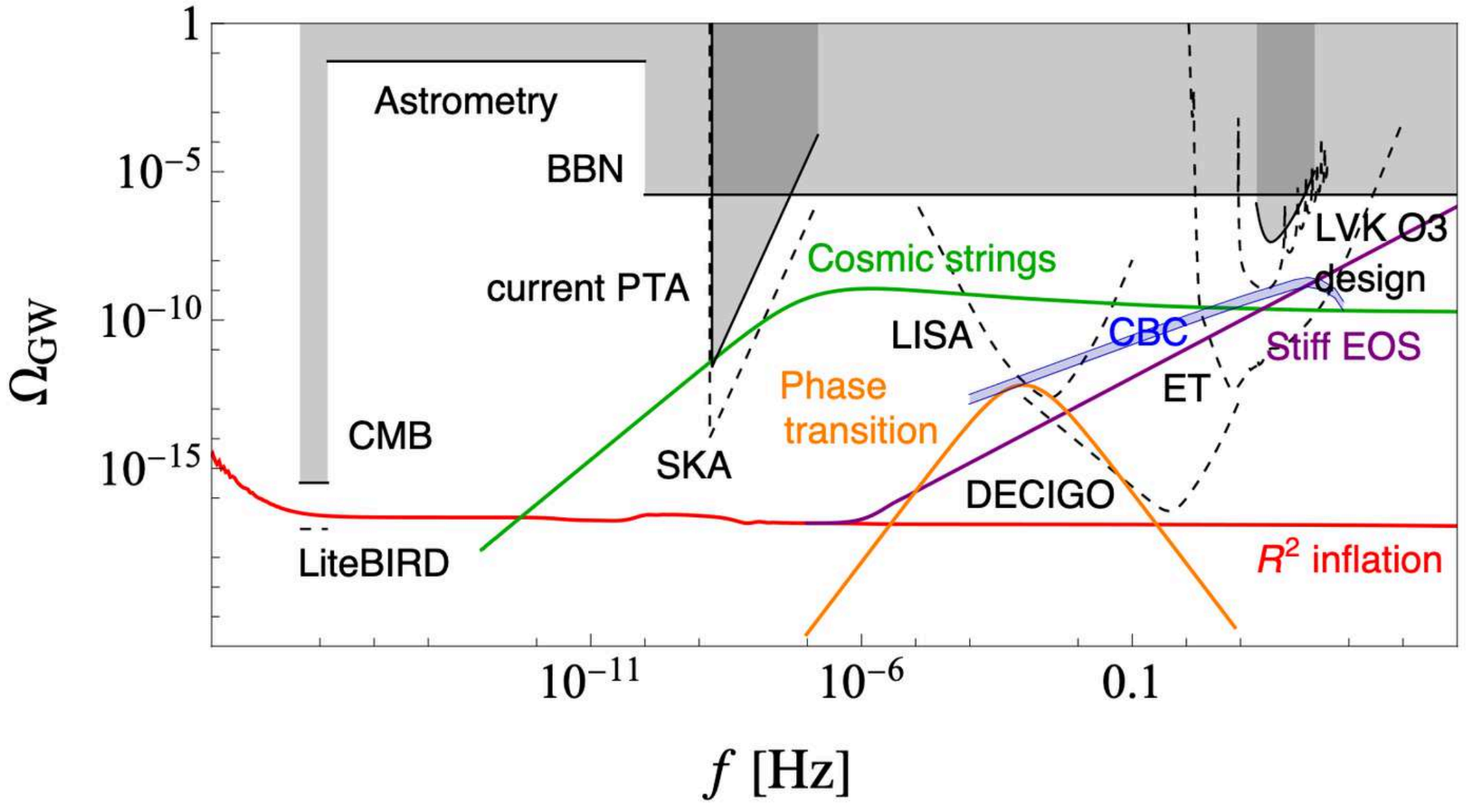
GWB characterization

Fractional energy density spectrum in GWs

$$\Omega_{\rm gw}(f) = \frac{1}{\rho_c}\frac{d\rho_{\rm gw}}{d\ln f}$$

$$\rho_{\rm GW} = \frac{c^2}{32\pi G}\langle \dot{h}_{ab}(t,\mathbf{x})\dot{h}^{ab}(t,\mathbf{x})\rangle$$

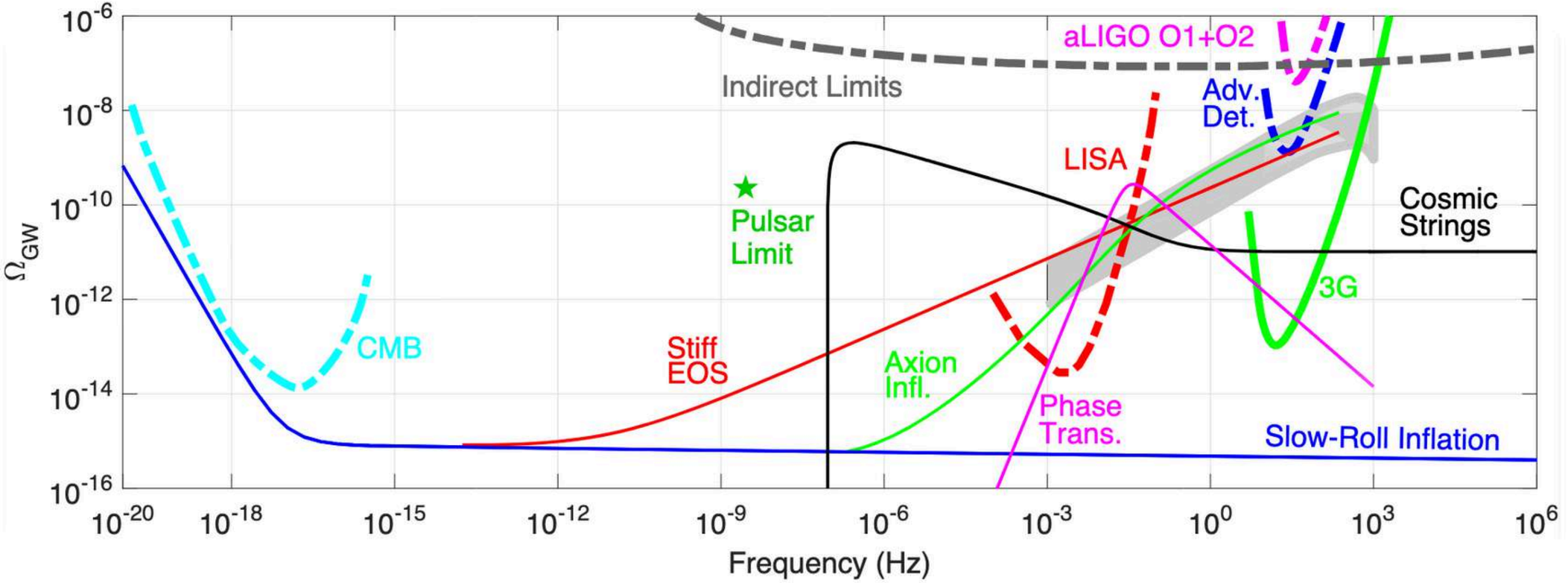
$$\Omega_{\rm GW}(f) = \frac{2\pi^2}{3H_0^2} f^3 S_h(f)$$



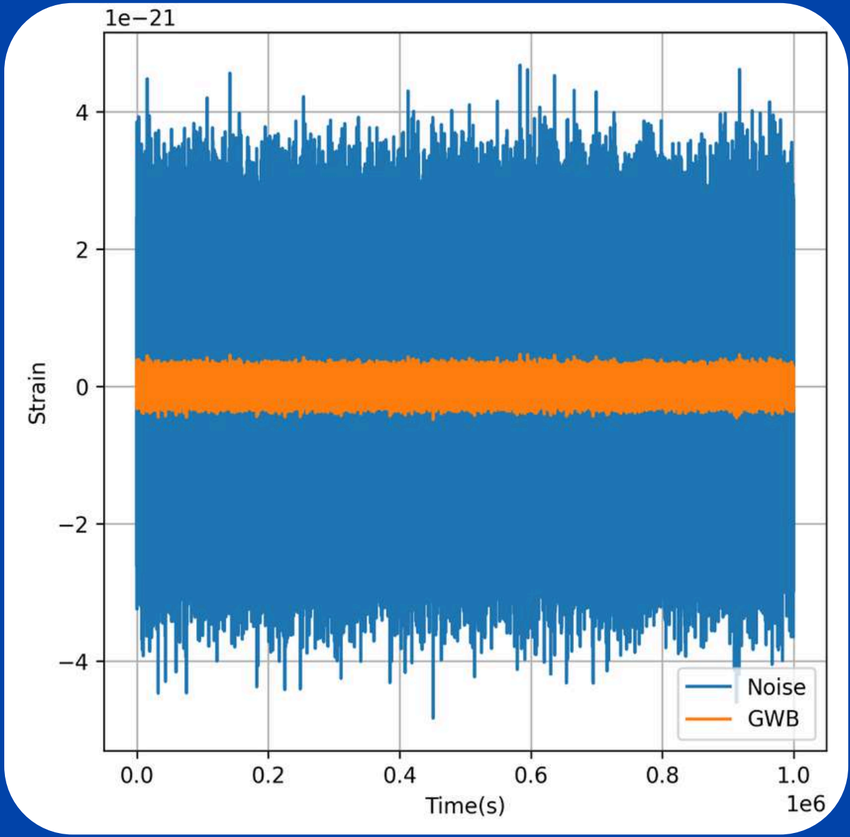
ARR, and S. Kuroyanagi. 2024. *Primordial Black Holes.* Chap. 27. Springer (link). Arxiv: https://doi.org/10.48550/arXiv.2407.00205.

LVK search for an isotropic GWB

Hybrid search → Frequentist
Hybrid search → Bayesian



LVK search for an isotropic GWB

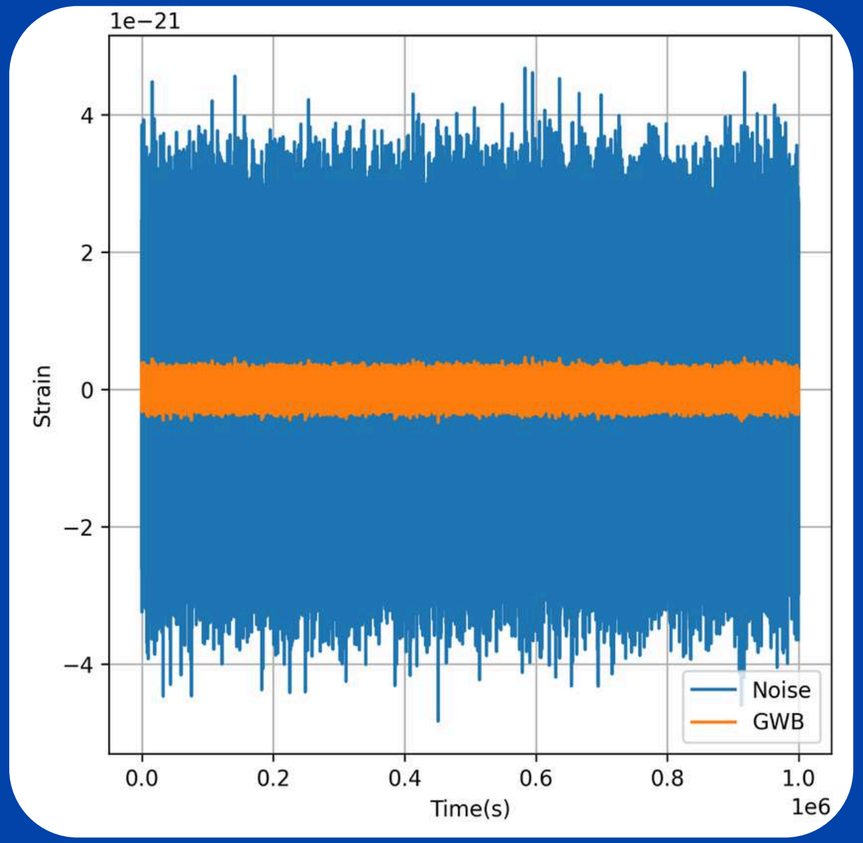


Cross correlation search

$$s_1(t) = n_1(t) + h_1(t),$$
$$s_2(t) = n_2(t) + h_2(t)\,.$$

$$\left\langle s_1^*(f)\, s_2(f') \right\rangle$$

LVK search for an isotropic GWB



Cross correlation search

$$s_1(t) = n_1(t) + h_1(t),$$
$$s_2(t) = n_2(t) + h_2(t)\,.$$

$$\langle s_1^*(f)\, s_2(f') \rangle$$

$$\langle n_i^*(f)\, h_j(f') \rangle = 0$$

$$\langle n_i^*(f)\, n_j(f') \rangle = \delta_{ij}$$

LVK search for an isotropic GWB

$$\langle s_1^*(f) s_2(f') \rangle$$

Cross correlation estimator and variance

$$\hat{C}^{IJ}(f) = \frac{2}{T} \frac{\mathrm{Re}[\tilde{s}_I^\star(f)\tilde{s}_J(f)]}{\gamma_{IJ}(f) S_0(f)}$$

$$\sigma^2_{IJ}(f) \approx \frac{1}{2T\Delta f} \frac{P_I(f) P_J(f)}{\gamma^2_{IJ}(f) S_0^2(f)}$$

LVK search for an isotropic GWB

Cross correlation spectrum (frequentist analysis)

$$\hat{C}^{IJ}(f) = \frac{2}{T} \frac{\mathrm{Re}[\tilde{s}_I^\star(f)\tilde{s}_J(f)]}{\gamma_{IJ}(f)S_0(f)}$$

$$\sigma^2_{IJ}(f) \approx \frac{1}{2T\Delta f} \frac{P_I(f)P_J(f)}{\gamma^2_{IJ}(f)S_0^2(f)}$$



LVK search for an isotropic GWB

Cross correlation spectrum (frequentist analysis)

$$\hat{C}^{IJ}(f) = \frac{2}{T} \frac{\mathrm{Re}[\tilde{s}_I^\star(f)\tilde{s}_J(f)]}{\gamma_{IJ}(f)S_0(f)}$$

$$\sigma^2_{IJ}(f) \approx \frac{1}{2T\Delta f} \frac{P_I(f)P_J(f)}{\gamma^2_{IJ}(f)S_0^2(f)}$$

T : observation time

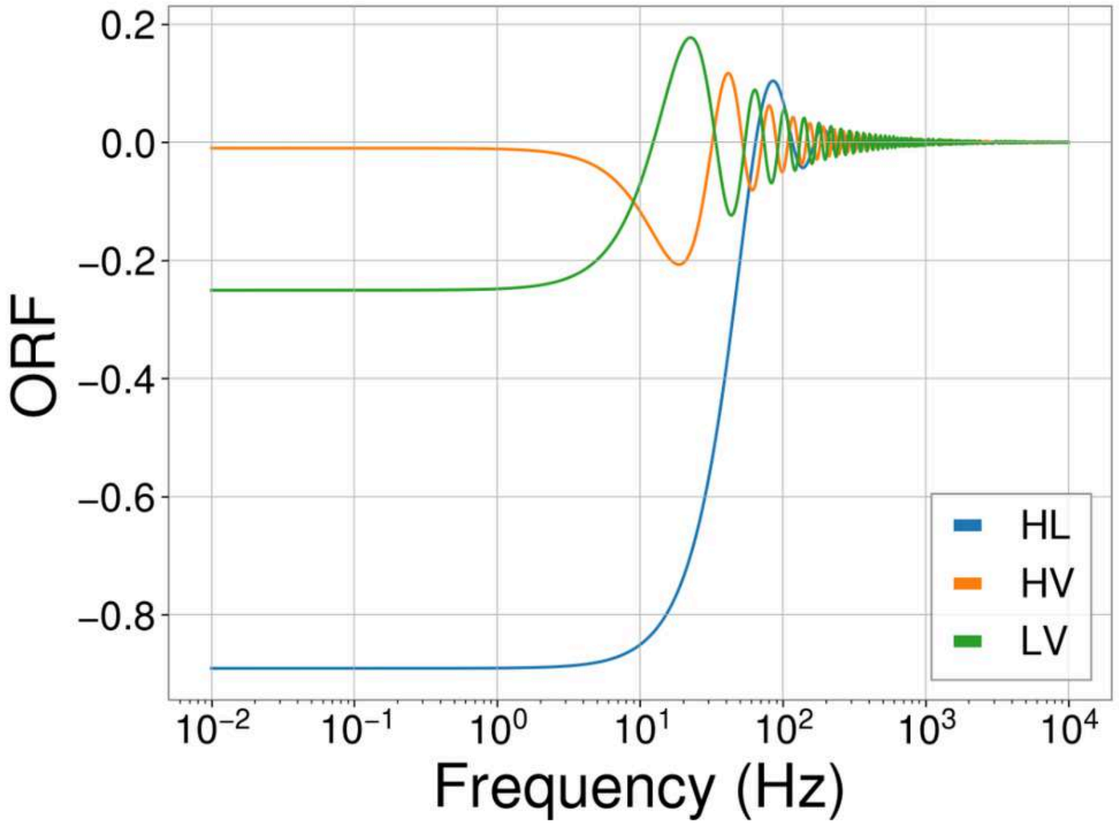
LVK search for an isotropic GWB

Cross correlation spectrum (frequentist analysis)

$$\hat{C}^{IJ}(f) = \frac{2}{T}\frac{\mathrm{Re}[\tilde{s}_I^{\star}(f)\tilde{s}_J(f)]}{\gamma_{IJ}(f)S_0(f)}$$

$$\sigma^2_{IJ}(f) \approx \frac{1}{2T\Delta f}\frac{P_I(f)P_J(f)}{\gamma^2_{IJ}(f)S_0^2(f)}$$

Overlap reduction function (ORF)

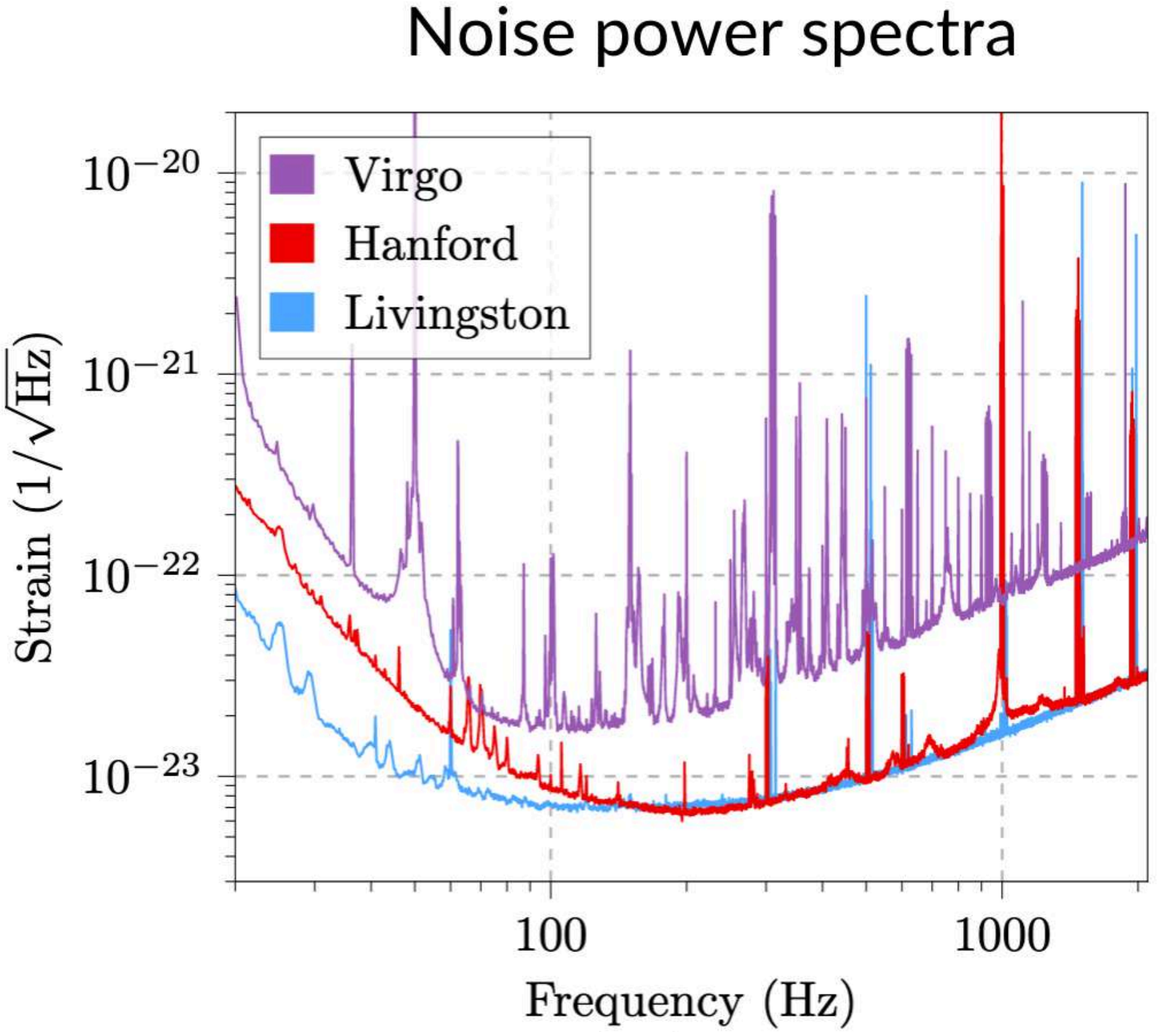


LVK search for an isotropic GWB

Cross correlation spectrum (frequentist analysis)

$$\hat{C}^{IJ}(f) = \frac{2}{T}\frac{\mathrm{Re}[\tilde{s}_I^{\star}(f)\tilde{s}_J(f)]}{\gamma_{IJ}(f)S_0(f)}$$

$$\sigma^2_{IJ}(f) \approx \frac{1}{2T\Delta f}\frac{P_I(f)P_J(f)}{\gamma^2_{IJ}(f)S_0^2(f)}$$



B. P. Abbott et al. (LVK), Phys. Rev. Lett. 119, 141101

LVK search for an isotropic GWB

Gaussian likelihood

$$p(\hat{\Omega}_0|\Theta,\Lambda) \propto \exp\left[-\frac{1}{2}\sum_f \frac{(\hat{\Omega}_0(f)-\Lambda\Omega_{\rm GW}(f;\Theta))^2}{\sigma_0^2(f)}\right]$$

LVK search for an isotropic GWB

Gaussian likelihood

$$p(\hat{\Omega}_0|\Theta,\Lambda) \propto \exp\left[-\frac{1}{2}\sum_f \frac{(\hat{\Omega}_0(f) - \Lambda\Omega_{\rm GW}(f;\Theta))^2}{\sigma_0^2(f)}\right]$$

Frequentist results

LVK search for an isotropic GWB

Gaussian likelihood

$$p(\hat{\Omega}_0|\Theta,\Lambda) \propto \exp\left[-\frac{1}{2}\sum_f \frac{(\hat{\Omega}_0(f) - \Lambda\Omega_{\rm GW}(f;\Theta))^2}{\sigma_0^2(f)}\right]$$

Frequentist versus Bayesian analyses: Cross-correlation as an approximate sufficient statistic for LIGO-Virgo stochastic background searches

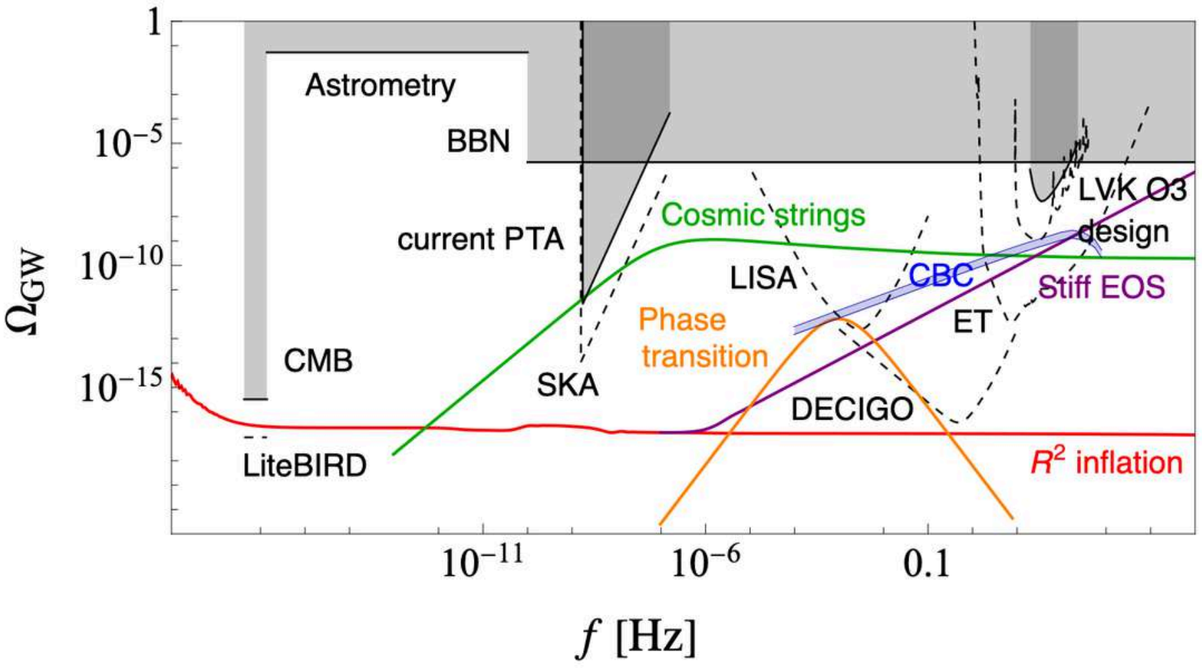
AM and JR, Phys. Rev. D 103, 062003

LVK search for an isotropic GWB

Gaussian likelihood

$$p(\hat{\Omega}_0|\Theta,\Lambda) \propto \exp\left[-\frac{1}{2}\sum_f \frac{(\hat{\Omega}_0(f) - \Lambda\Omega_{\rm GW}(f;\Theta))^2}{\sigma_0^2(f)}\right]$$

Model assumed to describe the GWB

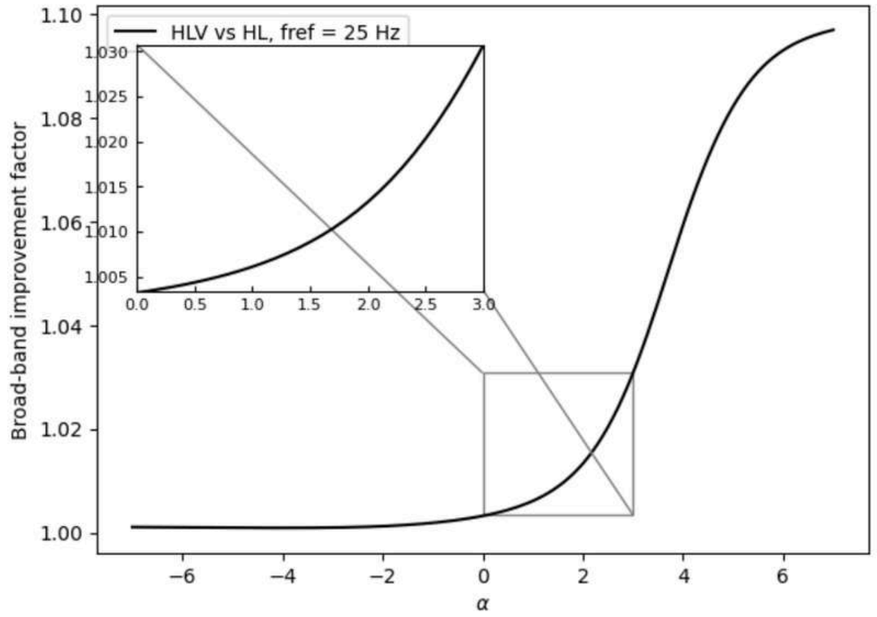


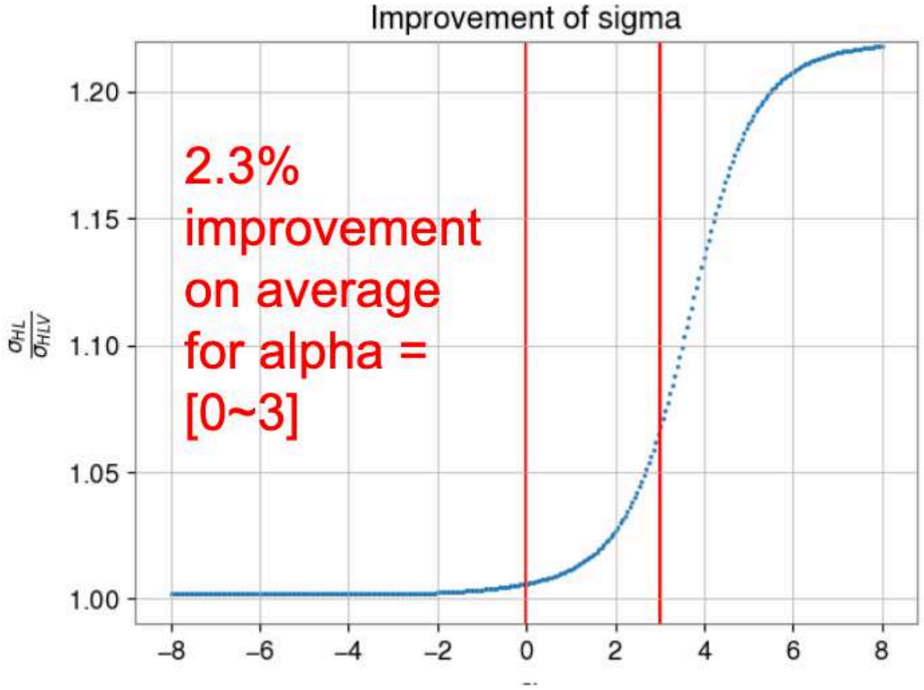
ARR, and S. Kuroyanagi. 2024. *Primordial Black Holes*. Chap. 27. Springer (link). Arxiv: https://doi.org/10.48550/arXiv.2407.00205.

Current LVK results

- H1, L1 data from O1-O4c1
- No Virgo data was used:
  - Theoretical assessment: broad-band improvement factors are marginal for:
    - α = 0: 1.003 (0.3%)
    - α = 2/3: 1.005 (0.5%)
    - α = 3: 1.031 (3%)
    - α ≥ 5: improvements ≥5% (10% for α = 7)
  - Data (O4b) driven assessment: marginal improvement in sensitivity

$$\Omega_{\mathrm{GW}}(f) = \Omega_{\mathrm{ref}} \left(\frac{f}{25\,\mathrm{Hz}} \right)^{\alpha}$$

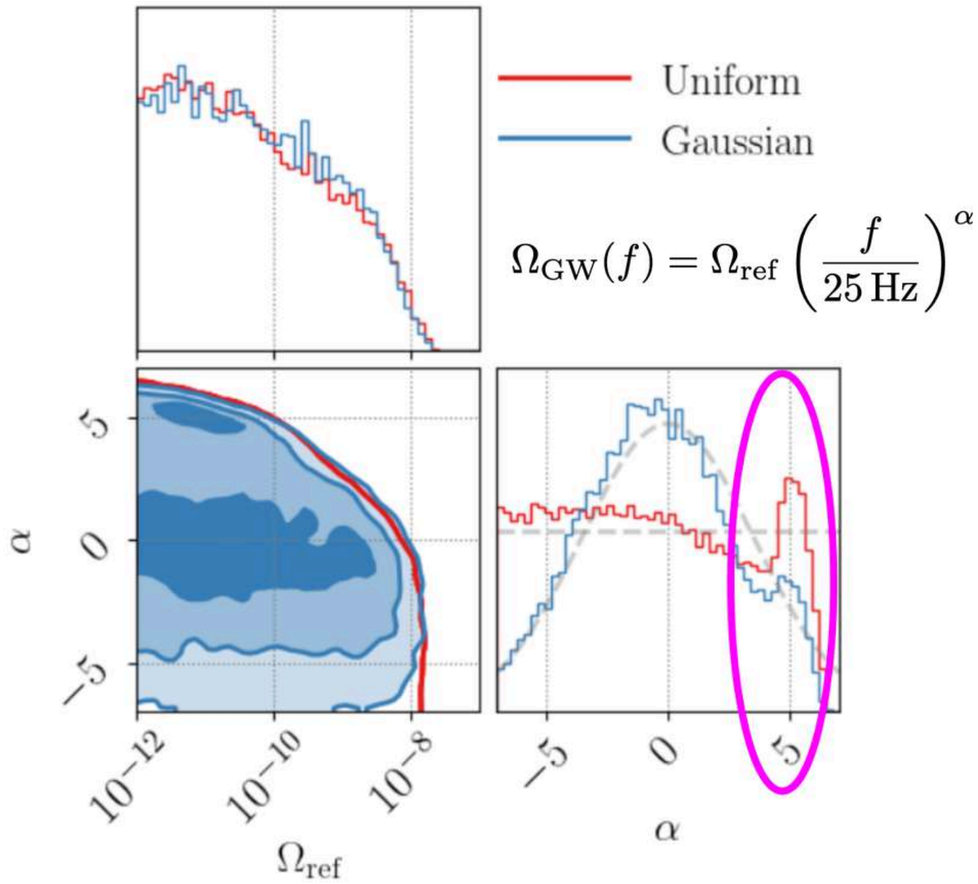




Current LVK results - data quality

New DQ issues not identified by standard tools:

- Peak in the α-posterior (first observed during O4a). Sources:
  - Narrowband 30 Hz and 100 Hz combs at Hanford (source identified: link)
  - Broadband artifact consistent with powerline harmonics in the 600–850 Hz band
  - Possible coupling/transient features in the 770–790 Hz range
  - Frequency regions with the largest contributions > 600 Hz

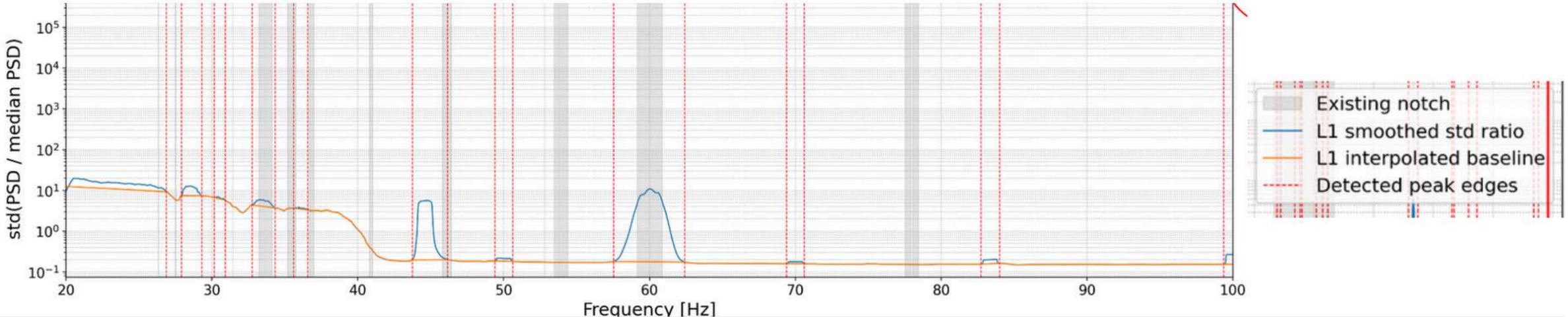


LVK Collaboration, arXiv:2508.20721 (2025)

Current LVK results - data quality

- New DQ issues addressed with a method based on temporal variability of the PSD.
- Frequencies with excess temporal variability relative to nearby frequencies (by more than a factor 1.5) are added to the notch list

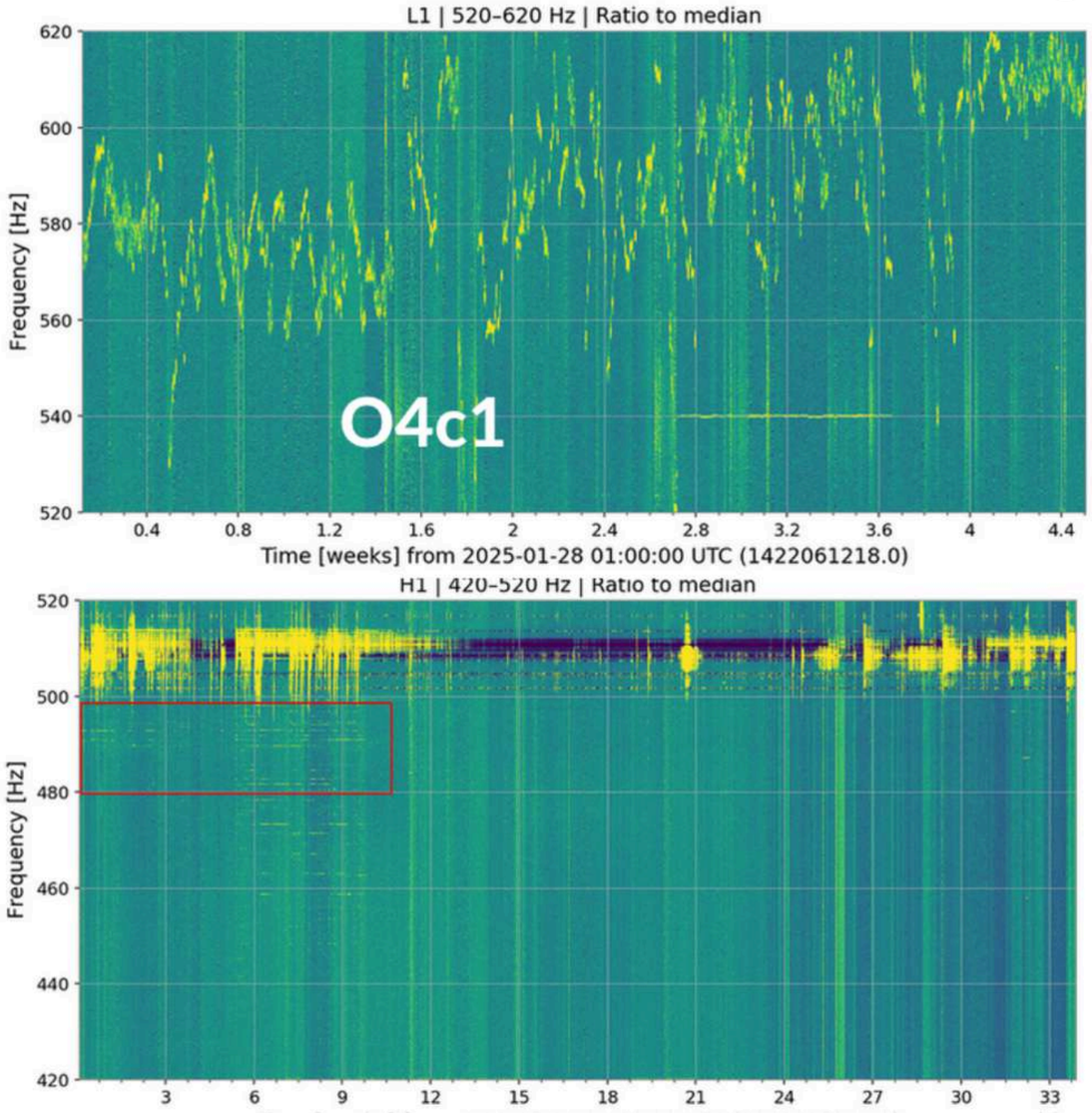
$$\mathrm{StdRatio}(f) = \mathrm{std}\left(\frac{\mathrm{PSD}(f)}{\mathrm{median}(\mathrm{PSD}(f))}\right)$$



Current LVK results - data quality

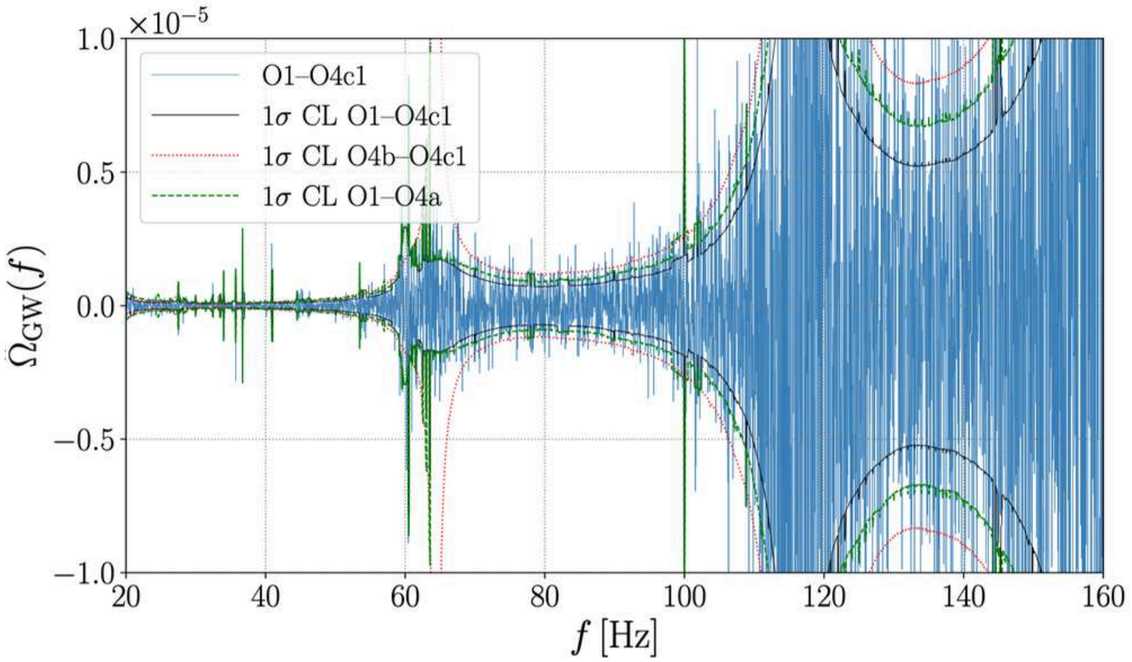
This procedure led to:

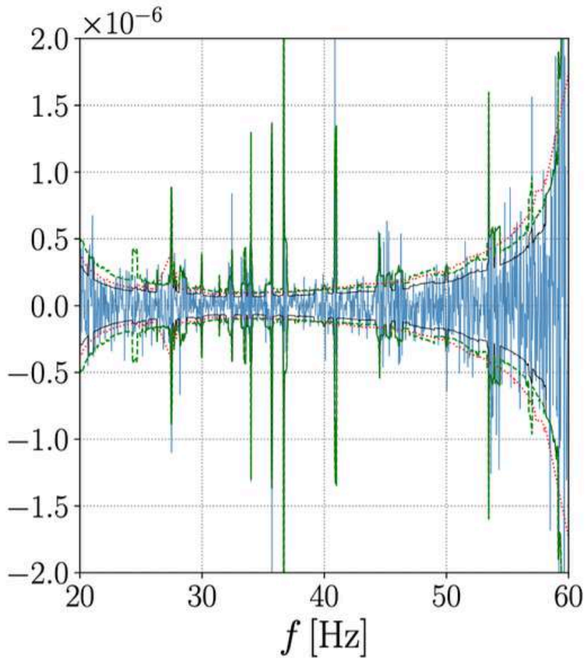
- Widening of notches around 60 Hz power-line harmonics
- Reduction of noise in the low-frequency region (< 100 Hz)
- Removal of noise in the high-frequency region (400–900 Hz):
  - Excess narrowband structures around the violin modes (~500 Hz)
  - Broadband, time-dependent excess in L1 between 540–640 Hz



Current LVK results

- Total coincident time ~ 140.99 days → 117.05 days of viable data after DQ cuts
- Frequency range of analysis: 20-1726Hz
- Pipeline: pygwb (A. R. et al 2023 ApJ 952 25)



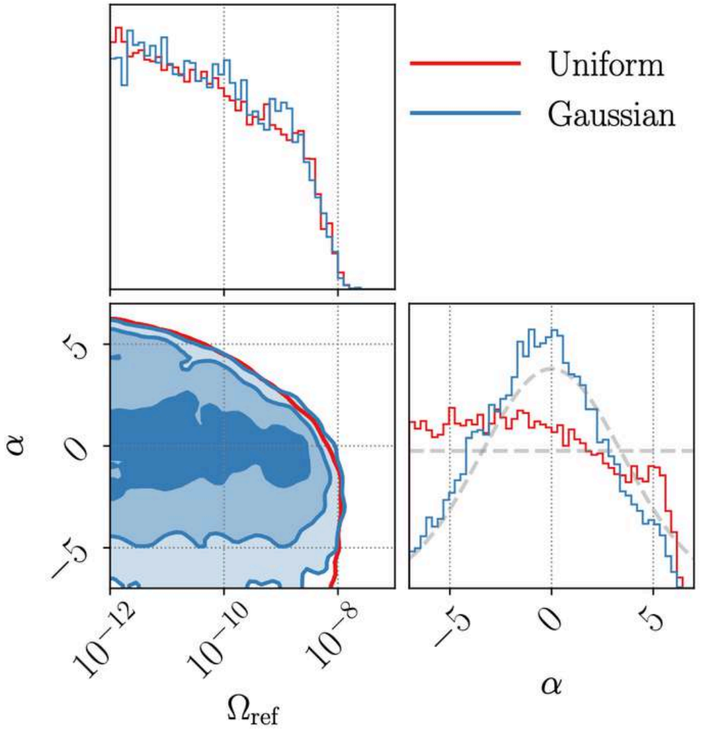


α	$f_{99\%}^{\rm O1-O4a}$ [Hz]	$\hat{\Omega}^{\rm O1-O4a}/10^{-9}$	$f_{99\%}^{\rm O4b-O4c1}$ [Hz]	$\hat{\Omega}^{\rm O4b-O4c1}/10^{-9}$	$f_{99\%}^{\rm O1-O4c1}$ [Hz]	$\hat{\Omega}^{\rm O1-O4c1}/10^{-9}$
0	64.7	1.1 ± 4.8	53.3	0.3 ± 4.9	56.2	0.7 ± 3.4
2/3	87.6	0.4 ± 3.6	84.2	-0.1 ± 3.9	86.3	0.2 ± 2.6
3	329.9	-0.3 ± 0.6	347.9	-0.3 ± 0.7	338.2	-0.3 ± 0.5

LVK Collaboration, arXiv:2608.23477 (2026)

Current LVK results - Bayesian

$$\Omega_{\rm GW}(f) = \Omega_{\rm ref} \left(\frac{f}{25\,\mathrm{Hz}} \right)^{\alpha}$$



Upper limits at 95% CL

	Uniform prior			Log-uniform prior		
α	O1–O4c1	O1–O4a	Improvement	O1–O4c1	O1–O4a	Improvement
0	7.4×10^{-9}	1.1×10^{-8}	1.5	2.8×10^{-9}	3.9×10^{-9}	1.4
2/3	5.5×10^{-9}	7.9×10^{-9}	1.4	2.0×10^{-9}	2.8×10^{-9}	1.4
3	7.5×10^{-10}	1.0×10^{-9}	1.3	2.6×10^{-10}	3.6×10^{-10}	1.4
Marginalized	1.1×10^{-8}	1.7×10^{-8}	1.5	2.7×10^{-9}	4.1×10^{-9}	1.5

LVK Collaboration, arXiv:2608.23477 (2026)

Current LVK results - constraints on non-GR pols

- Signal may include vector, scalar and tensor polarizations
- No evidence for such a signal → ULs
- Model: mixed background

$$\Omega_{\mathrm{GW}}(f;\Theta) = \sum_{(\mathrm{p})} \beta^{(\mathrm{p})}(f)\Omega^{(\mathrm{p})}_{\mathrm{ref}} F_{\alpha_{\mathrm{p}}}(f)$$

$$\beta^{(\mathrm{p})}(f) \equiv \gamma^{(\mathrm{p})}_{IJ}(f)/\gamma_{IJ}(f)$$

Current LVK results - constraints on non-GR pols

- Signal may include vector, scalar and tensor polarizations
- No evidence for such a signal → ULs
- Model: mixed background

$$\Omega_{\rm GW}(f;\Theta) = \sum_{\rm (p)} \beta^{\rm (p)}(f)\Omega^{\rm (p)}_{\rm ref} F_{\alpha_{\rm p}}(f)$$

$$\beta^{\rm (p)}(f) \equiv \gamma^{\rm (p)}_{IJ}(f)/\gamma_{IJ}(f)$$

- ULs at 95% CL:

Polarization	O1−O4c1	Improvement
Tensor	2.7×10^{-9}	1.5
Vector	2.7×10^{-9}	1.4
Scalar	6.9×10^{-9}	1.3

- Signal versus noise Bayes factor:

$$\log_{10}\mathcal{B} = -0.947 \pm 0.004$$

- Non-GR vs GR Bayes factor:

$$\log_{10}\mathcal{B} = -0.498 \pm 0.010$$

LVK Collaboration, arXiv:2608.23477 (2026)

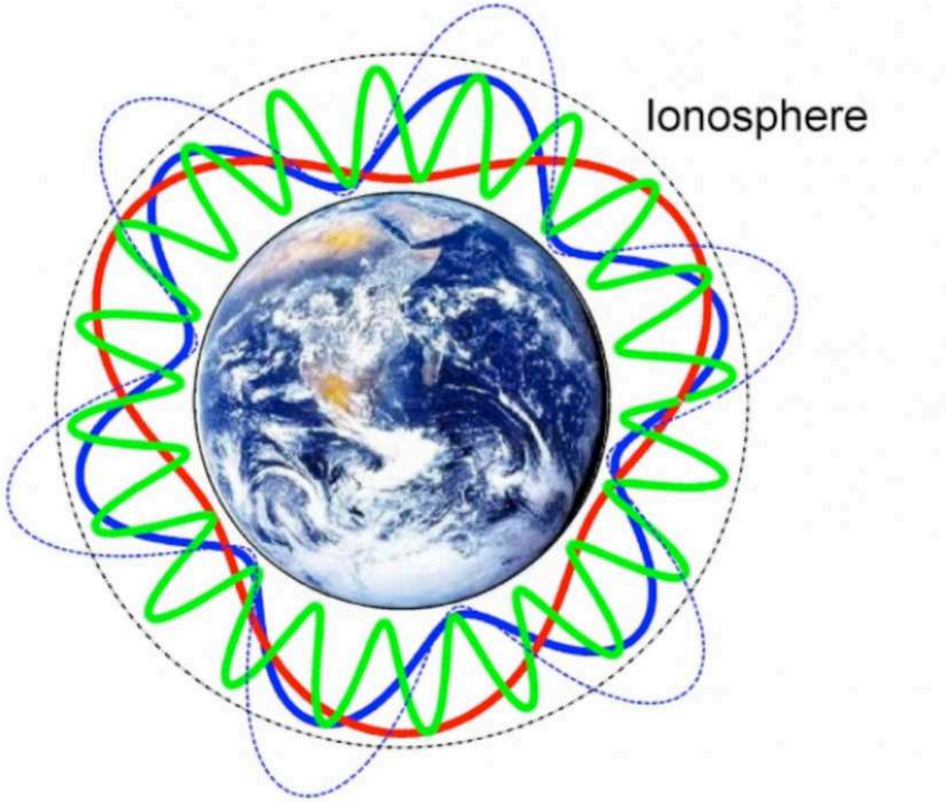
Current LVK results - magnetic budget

- Correlated magnetic noise:
  - Electronic mains
  - Synchronisation to GPS
  - Schumann resonances

$$\langle n_i^*(f) n_j(f') \rangle = \delta_{ij}$$

Current LVK results - magnetic budget

- Correlated magnetic noise:
  - Electronic mains
  - Synchronisation to GPS
  - Schumann resonances



Current LVK results - magnetic budget

$$\hat{\Omega}_{\mathrm{mag},\,IJ}(f) = \frac{2}{T}\frac{|T_I(f)|\,|T_J(f)|\,\sqrt{\sum_{ab}|\tilde{m}^{\star}_{I,a}(f)\tilde{m}_{J,b}(f)|^2}}{\gamma_{IJ}(f)S_0(f)}$$

Current LVK results - magnetic budget

$$\hat{\Omega}_{\mathrm{mag},\,IJ}(f) = \frac{2}{T}\frac{|T_I(f)|\,|T_J(f)|\sqrt{\sum_{ab}|\tilde{m}^{\star}_{I,a}(f)\tilde{m}_{J,b}(f)|^2}}{\gamma_{IJ}(f)S_0(f)}$$

- mI,a(f): FTed magnetic data from the magnetic data of detector I

Current LVK results - magnetic budget

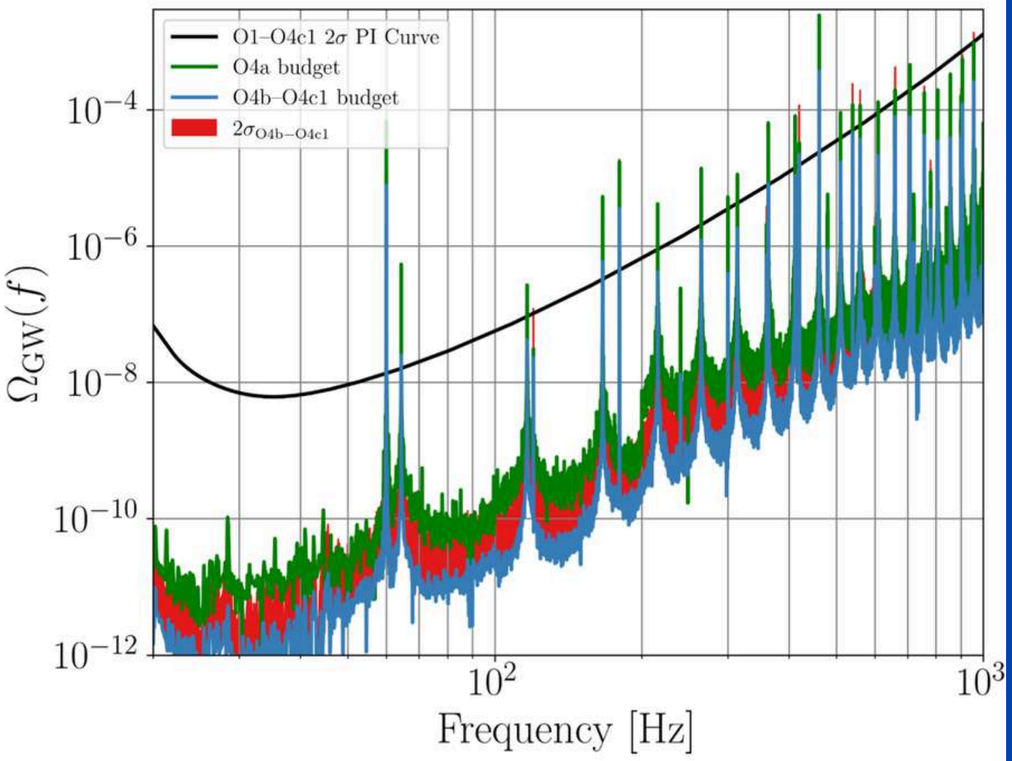
$$\hat{\Omega}_{\mathrm{mag},\,IJ}(f) = \frac{2}{T}\frac{|T_I(f)||T_J(f)|\sqrt{\sum_{ab}|\tilde{m}^{\star}_{I,a}(f)\tilde{m}_{J,b}(f)|^2}}{\gamma_{IJ}(f)S_0(f)}$$

- mI,a(f): FTed magnetic data from the magnetic data of detector I
- TI (f): magnetic coupling function of detector I

Current LVK results - magnetic budget

$$\hat{\Omega}_{\mathrm{mag},\,IJ}(f) = \frac{2}{T}\frac{|T_I(f)|\,|T_J(f)|\sqrt{\sum_{ab}|\tilde{m}^{\star}_{I,a}(f)\tilde{m}_{J,b}(f)|^2}}{\gamma_{IJ}(f)S_0(f)}$$

- mI,a(f): FTed magnetic data from the magnetic data of detector I
- TI (f): magnetic coupling function of detector I



LVK Collaboration, arXiv:2608.23477 (2026)

LVK results - astrophysical implications

$$R_{\rm BBH}(z) = C(\alpha_z, \beta_z, z_{\rm p}) \frac{R_0 (1+z)^{\alpha_z}}{1 + \left(\frac{1+z}{1+z_{\rm p}}\right)^{\alpha_z + \beta_z}}$$

energy spectrum emitted by a single binary evaluated in terms of the source frequency

$$\Omega_{\rm GW}(f;\theta_k) = \frac{f}{\rho_c H_0} \int_0^{z_{\rm max}} dz \frac{R_m(z;\theta_k) \left\langle \frac{dE_{\rm GW}}{df_s}(f_s;\theta_k) \right\rangle}{(1+z) E(\Omega_{\rm m,0}, \Omega_{\Lambda,0}, z)}$$

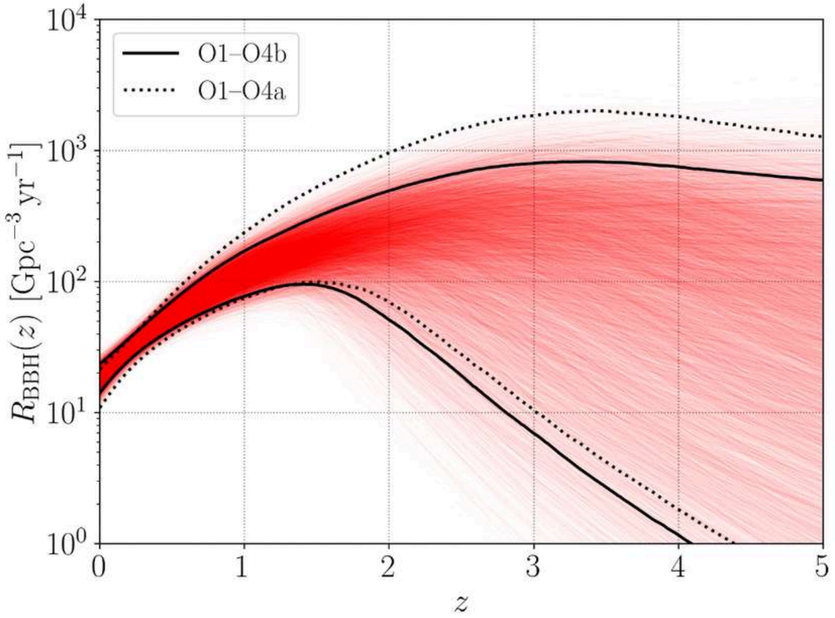
accounts for the dependence of co-moving volume on cosmology

LVK Collaboration, arXiv:2608.23477 (2026)

LVK results - astrophysical implications

Present-day merger rate is inferred to be:

BBH	$18.4^{+5.1}_{-4.2}\,\mathrm{Gpc}^{-3}\mathrm{yr}^{-1}$
BNS	$38^{+69}_{-30}\,\mathrm{Gpc}^{-3}\mathrm{yr}^{-1}$
NSBH	$22^{+24}_{-14}\,\mathrm{Gpc}^{-3}\mathrm{yr}^{-1}$



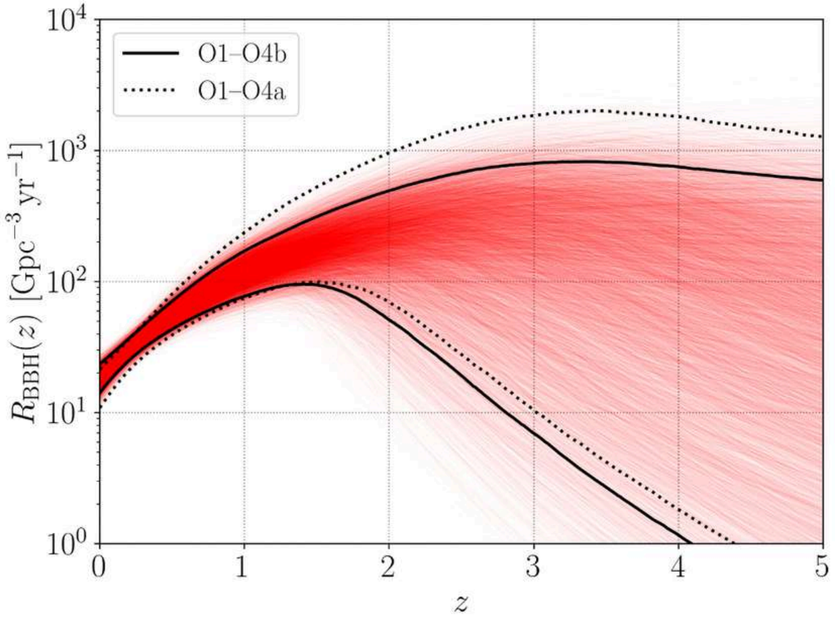
LVK Collaboration, arXiv:2608.23477 (2026)

LVK results - astrophysical implications

Present-day merger rate is inferred to be:

BBH	$18.4^{+5.1}_{-4.2}\,\mathrm{Gpc}^{-3}\mathrm{yr}^{-1}$
BNS	$38^{+69}_{-30}\,\mathrm{Gpc}^{-3}\mathrm{yr}^{-1}$
NSBH	$22^{+24}_{-14}\,\mathrm{Gpc}^{-3}\mathrm{yr}^{-1}$

Consistent with pops. analysis results



LVK Collaboration, arXiv:2608.23477 (2026)

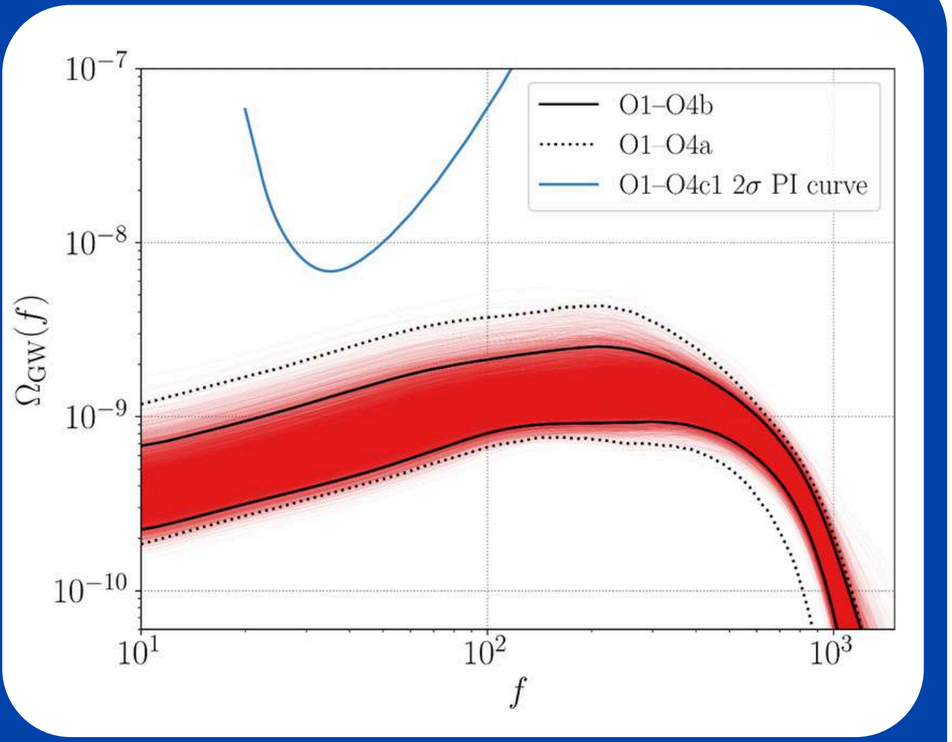
LVK results - astrophysical implications

- Using rejection sampling:

$$p(\hat{\Omega}_0, \{d_i\}|\Lambda_{\rm BBH}) = p_{\rm BBH}(\{d_i\}|\Lambda_{\rm BBH}) \times p_{\rm stoch}(\hat{\Omega}_0|\Lambda_{\rm BBH})$$

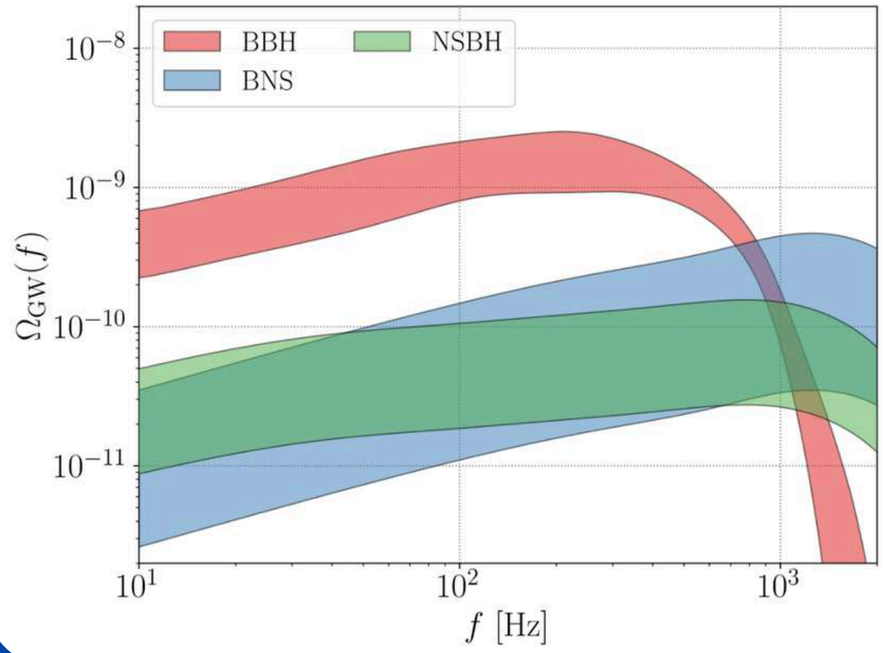
- Upper bound is reduced by ~ x2 (improved constraints on the BBH merger-rate density)
- Estimated amplitude at 25 Hz:

$$\Omega_{\rm BBH}(25\,{\rm Hz}) = 5.6^{+5.0}_{-2.1} \times 10^{-10}$$



LVK Collaboration, arXiv:2608.23477 (2026)

LVK results - astrophysical implications



$$\Omega_{\rm BBH}(25\,{\rm Hz}) = 5.6^{+5.0}_{-2.1}\times10^{-10}$$

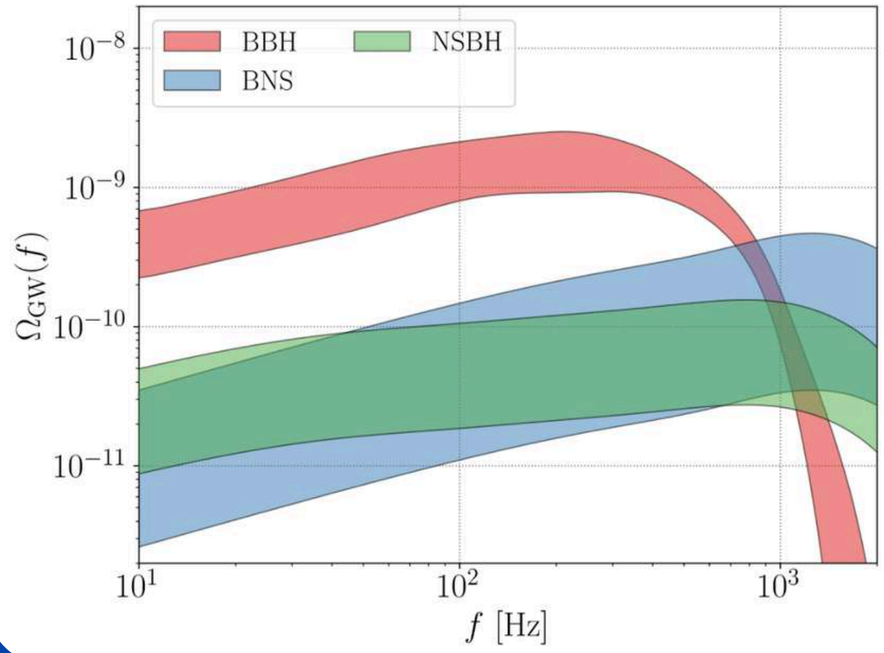
$$\Omega_{\rm BNS}(25\,{\rm Hz}) = 2.3^{+4.1}_{-1.8}\times10^{-11}$$

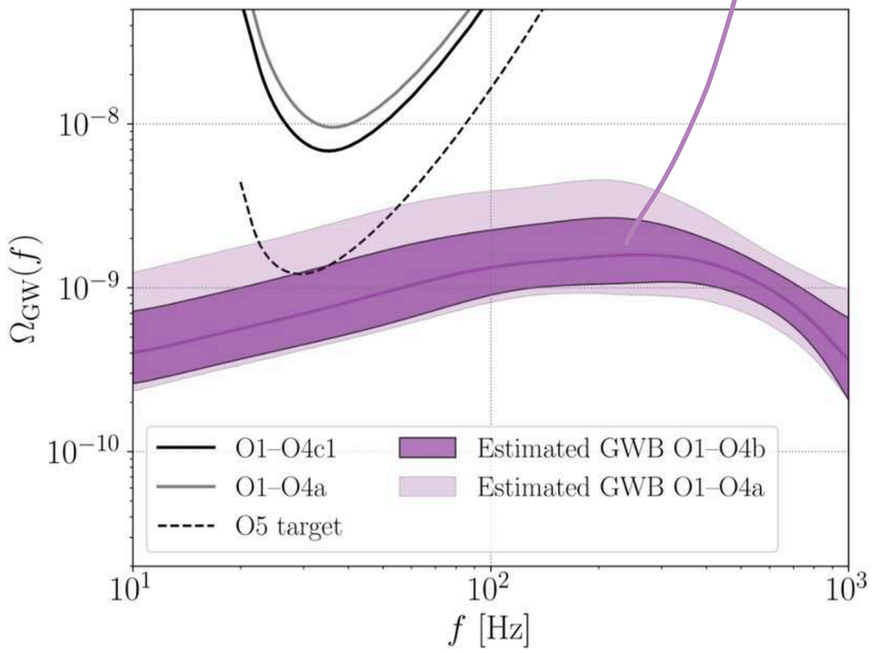
$$\Omega_{\rm NSBH}(25\,{\rm Hz}) = 3.6^{+4.0}_{-2.3}\times10^{-11}$$

LVK Collaboration, arXiv:2608.23477 (2026)

LVK results - astrophysical implications

$$\Omega_{\rm CBC}(25\,{\rm Hz}) = 6.3^{+5.0}_{-2.2} \times 10^{-10}$$



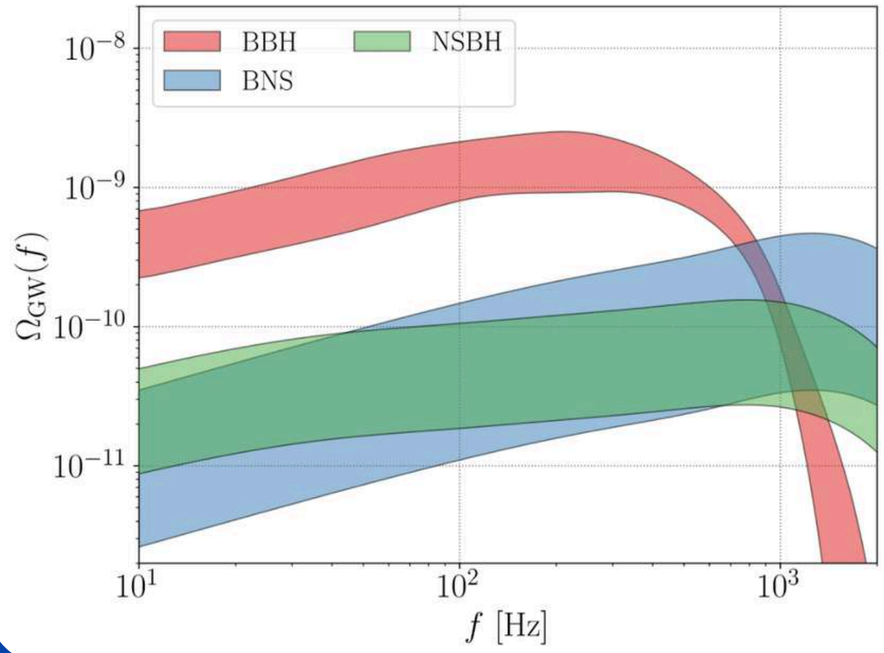


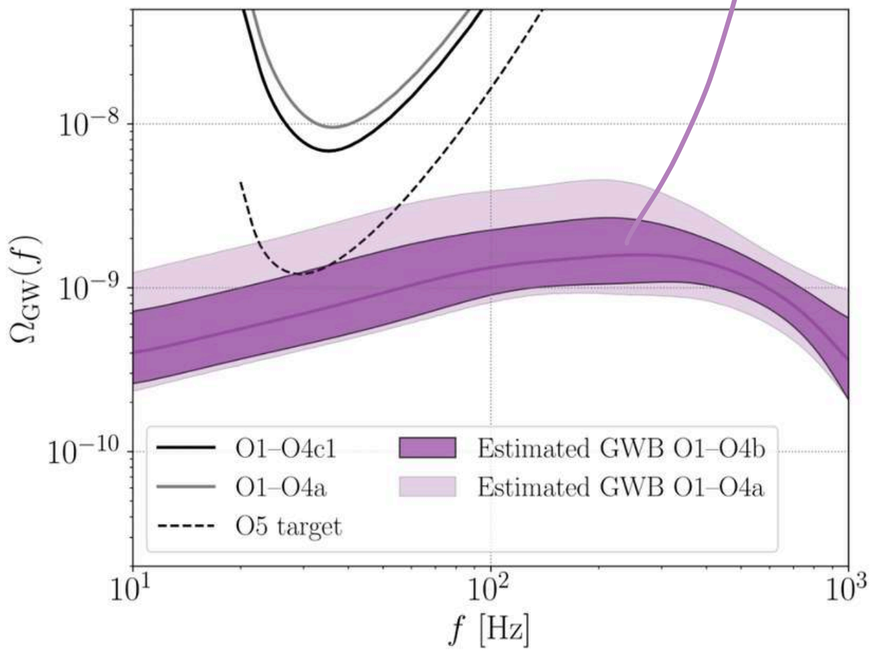
LVK Collaboration, arXiv:2608.23477 (2026)

LVK results - astrophysical implications

Detectable in A+?

$$\Omega_{\rm CBC}(25\,{\rm Hz}) = 6.3^{+5.0}_{-2.2} \times 10^{-10}$$

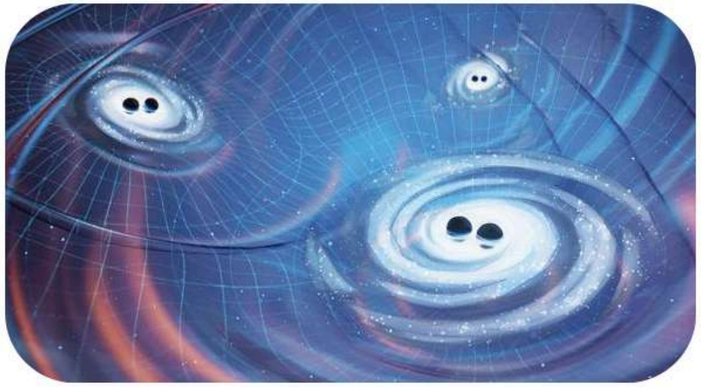




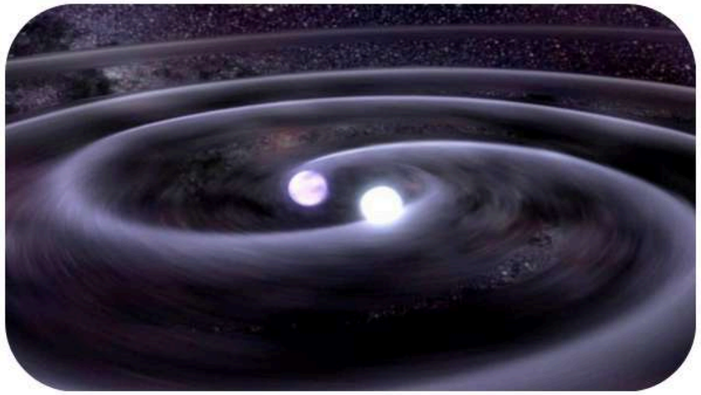
LVK Collaboration, arXiv:2608.23477 (2026)

Summary

- GWTC-5 and CBC population properties:
  - 161 new CBC candidates, bringing the total to 390
  - Several new events have high SNRs >30
  - The BBH mass distribution shows significant structure, including mass-dependent features
  - The BBH merger-rate evolution with redshift is consistent with the cosmic star-formation history
- Isotropic GWB search
  - H1, L1 data. V1 data excluded because of marginal improvement in sensitivity
  - New DQ challenges → solved with PSD variability
  - New notchlists for O4a, O4b and O4c1
  - No detected signal → we set updated ULs improved by x1.5
  - No correlated magnetic noise biasing our results
  - Feasible astrophysical foreground detection during O5







BACKUP